PhD degree in Systems Medicine

Curriculum in Human Genetics

European School of Molecular Medicine (SEMM),

University of Milan and University of Naples Federico II

Settore disciplinare: BIO/12

Intestinal microbiota is a major determinant in the response to oncolytic vaccines in a mouse model of melanoma

Lorella Tripodi

CEINGE-Biotecnologie Avanzate, Napoli

Matricola n. R12081

Supervisor: Prof. Lucio Pastore, CEINGE-Biotecnologie Avanzate, Napoli

Internal Supervisor: Prof. Francesco Salvatore, CEINGE-Biotecnologie Avanzate, Napoli

External Supervisor: Prof. Vincenzo Cerullo, University of Helsinki, Helsinki, Finland

Anno accademico 2020-2021

Table of contents

List of abbreviations alphabetic order

Antigen-presenting cell (APC); Cytotoxic T-lymphocyte antigen 4 (CTLA-4); Programmed cell death protein 1 (PD-1); Programmed death-ligand 1 (PD-L1); immune checkpoint inhibitors (ICIs); Oncolytic viruses (OVs); Ad5D24-CpG (Ad-CpG); Immune checkpoint inhibitors (ICIs); Bifidobacterium (Bifidus)

Figures index

1.ABSTRACT

Cancer immunotherapy has achieved tremendous results, however the outcome of therapies targeting immune inhibitory pathways, specifically CTLA-4 and the axis between programmed cell death protein 1 (PD-1) and its ligand 1 (PD-L1) has many genetic and environmental sources of variability. Many studies demonstrated the influence of gut microbiome on immune checkpoint inhibitors (ICIs) outcome. Besides ICIs, oncolytic vaccines (OVs) are a promising therapeutic alternative in cancer immunotherapy with possible relevant contribution to treatment of several types of tumors; OVs are, in fact, able to convert immunologically “cold” tumors into “hot” ones. OVs represent an optimum candidate to combine with ICIs, increasing their response blockade both in immunogenic and poorly immunogenic tumors. We hypothesized that manipulation of intestinal gut microbiota could also affect OVs therapeutic efficacy; at this aim, we determined whether efficacy of the oncolytic adenovirus Ad5D24-CpG (Ad-CpG) therapy could be affected by the gut microbiome in a syngeneic mouse model of melanoma. Sterilization of the gut microbiota with high-dose vancomycin impaired efficacy of Ad-CpG therapy, reducing the tumor-infiltrating IFN-gamma CD8 T-cell. Cohousing mice pre-treated with vancomycin and a control group, with consequent microbiota restoration, prior to treatment with Ad-CpG, ablated the negative effect of antibiotic, confirming that Ad-CpG-reduced efficacy was mediated by the intestinal microbiota.

Considering the ability of Bifidobacterium as a positive regulator of antitumor immunity in vivo, by promoting pro-inflammatory signals in innate immune cells, we evaluated tumor regression in syngeneic mouse model of melanoma treated with a combination of Ad-CpG and Bifidobacterium spp. cocktail. The group receiving the combined regimen showed the best tumor control and an enrichment of bacteria belong to Firmicutes phylum, evaluated by fecal microbiome profiling by 16S rRNA. Our data indicates that gut microbiota affects the immune responses elicited by oncolytic adenovirus Ad-CpG and Bifidobacterium supplementations maximize its activity.

2.INTRODUCTION

2.1 Skin cancer overview

The incidence of cutaneous melanoma has rapidly increased in the past decades and at present this tumor is the ninth most common malignancy and the second for mortality. Every year, there are nearly 100,000 new cases of melanoma in the United States, and about 9,000 patients die of this cancer (1). Despite prevention campaigns, melanoma incidence has increased at a faster rate compared to most other cancers, especially in young Caucasian women (2). Melanoma patients with distant metastases show a 5-year survival rate of 23%, making metastasis the leading cause of melanoma-associated deaths (3). Several factors are involved in the pathogenesis of melanoma, including environmental, genetic, and immunological ones (4). Some studies have revealed that many factors may favor the development of melanoma; among them, the exposure to ultraviolet (UV) rays play an important role (5). Genetics factors may have a role in the pathogenesis of melanoma; nearly 40-50% of cutaneous melanomas have mutations in BRAF, a gene that belongs to the family of mitogen activated protein kinase (MAPK) and codes for a serine/threonine protein kinase constituting part of RAS-RAF-MEK. (6). BRAF activation induces the phosphorylation of extracellular signal regulated kinases (ERK) that constitute the most common mutated isoforms in cancer. The most common mutation is the V600E; in some cases, another mutation of BRAF named V600K has been described (7). Some other gene mutations have been described in studies such as NRAS and KIT. Therefore, studies have revealed that there is a high mutation rate in melanoma when comparing to other common tumors (8).

The increased tumor mutation burden (TMB) is at the base of the high immunogenicity of melanoma that is, therefore, sensitive to immunological therapies such as Immune checkpoint inhibitors (ICI) (4). Progression of melanoma is also due to a lack of activation of the immune system and the ability of the tumor to evade the immune system (immune escape). The immune system is able to control the disease only in the initial phase when defense mechanisms are still efficient; subsequently, the tumor itself causes immune system exhaustion for the continuous antigenic stimulation. Exhaustion of the immune system and the immune escape allow melanoma to grow and become metastatic (1,9). Melanoma cells can evade immune detection through a reduction of the expression of immunogenic tumor antigens, a reduction of the histocompatibility complex class I (MHC

I), alteration of the antigen process, recruitment of immunosuppressive cells such as Treg and suppressor cells derived from myeloid cells, and reduction of immunosuppressive molecules such as TGFß, Vascular-Endothelial Growth Factor (VEGF), adenosine, or Indoleamin 2,3-dioxygenase enzyme (IDO) (10-11).

2.2 Immunotherapy of melanoma using immune checkpoint inhibitors

The molecular mechanism of immunotherapy is based on the interaction between immune system and molecules present on the surface of cancer cells. The immune response against neoplasms is mainly mediated by the adaptive immune system and cytotoxic T-lymphocytes (CTL). In order to react against any foreign cell, naïve T-lymphocytes must be activated and thus cytotoxic response can be started via two signals: the first signal is mediated by T-cell receptor (TCR) connected to a specific antigen on an antigen-presenting cell (APC), and the secondary signal is based on the interaction between a CD28 receptor on lymphocyte surface and CD80/86 on APC (Figure 1). Progression of a correct immune response is characterized by immunological checkpoints that prevent unwanted and harmful self-directed activities that lead to autoimmunity (12). Therapies developed to overcome these mechanisms by blocking the inhibitory checkpoints allow generating antitumor activity alone and/or in combination with other therapies. In melanoma, these therapies target molecules that are pathologically overexpressed in melanoma such as PD-1 or CTLA-4 (13-14) as shown in Figure 1 and in Figure 2. In 1987, James P. Allison identified cytotoxic T-lymphocyte antigen 4 (CTLA-4) preventing T-cells from attacking tumor cells. He hypothesized that blockage of the CTLA4 would allow to active the immune system against cancer cell. CTLA-4, which is a member of the CD28 superfamily, is induced after CD28 binding and activation. B7-1 and B7-2 are the specific ligand of CTLA-4. Interaction between CTLA-4 and activated T-cells leads to another downregulation signal, blocking IL-2 transcription and, consequently, progression through the cell cycle (15). The highest effective molecule CTLA-4 blockade is currently Ipilimumab (16); several studies have shown promising results with this molecule and durability of the response, even when treatment was discontinued (17).

In the 1990s, Okazaki et al. discovered a molecule on T-cells, which was called programmed death-1 (PD-1). PD-1 is a cell-surface molecule with inhibitory properties expressed by activated T- and B-cells and natural killer lymphocytes that downregulates the effector function (18). Studies have proven increase in the expression of PD-1 in melanoma, which means a strong downregulation of activated T-cells that helps the maintenance of tumor cells. (19,20).

Nivolumab and Pembrolizumab target the interaction between PD-1 and its ligands PDL-1 and PDL-2; in melanoma, PDL-1 expression is enhanced by the presence of interferon-gamma-secreting lymphocytes from the microenvironment. Many trials have indicated clinical efficacy of Nivolumab and Pembrolizumab in melanoma especially in comparison with Ipilimumab (21). Almost 20 years later from Okazaky's discovery, the clinical data indicate that anti-PD1 immunoglobulins have been the most effective in melanoma.

So far, many antibodies have been approved for cancer treatment (e.g. rituximab, trastuzumab, alemtuzumab, avelumab). The first FDA-approved immunotherapies in metastatic/unresectable cutaneous melanomas, which are accountable for the vast majority of deaths caused by skin cancers, include anti-PD-1 drugs (nivolumab, pembrolizumab) and anti-CTLA-4 antibody ipilimumab. One of the new frontiers of immune checkpoint inhibition is the possibility to achieve long-term survival thanks to the memory of the immune system. In fact, immunotherapy tends to turn the tumor into a chronic disease in a percentage close to 20%; in a recent meta-analysis on nearly 5,000 patients with advanced melanoma treated with Ipilimumab, the authors showed that nearly 20% of the patients survived over 10 years (22).

Despite the impact of ICIs in cancer therapy, accumulating evidence suggest some critical limitations: firstly some patients undergoing ICIs therapy experience severe immune-related adverse events (23); secondly only a fraction of cancer patients benefit from ICI treatment and, lastly, ICIs are ineffective against tumors characterized by a low tumor-infiltrating lymphocyte (TIL) count (24) identified as immunologically "cold" tumors. To this end, OVs, that preferentially infect and lyse cancer cells, have been proposed as a promising modality for combination therapy to address the limitations of ICIs . This is due to the unique ability of OVs to inflame a "cold" tumor microenvironment (TME) into a "hot" environment with increased immune cells and lymphocyte infiltration, making them an ideal candidate for combination with various cancer immuno-therapeutics (24,25). For this

reason, multiple ongoing clinical trials are aiming to investigate the combined therapeutic efficacy of ICIs and OVs.

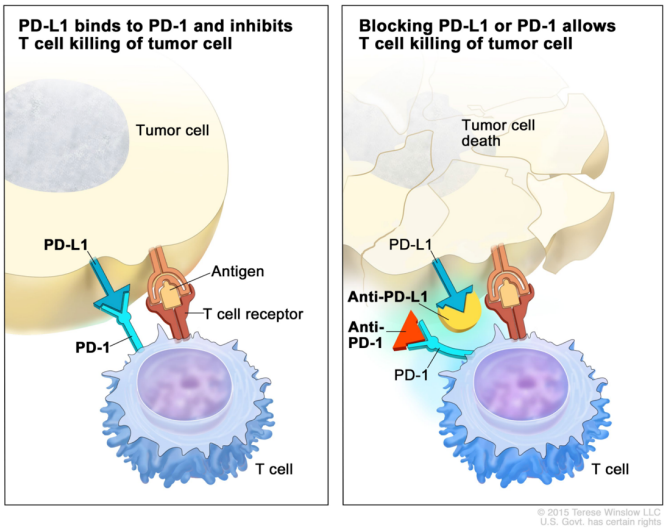

Figure 1. Mechanism of action of PD-1 and -D-L1 inhibitors. Tumor cells develop PD-L1 to bind with PD-1 on T-cells, which prevents T-cells from destroying the tumor cells (left). By blocking the ability of PD-L1 to bind to PD-1 with a PD-1 or PD-L1 inhibitor, T-cells are then able to kill the tumor cells (right). PD-1 = programmed cell death protein 1; PD-L1 = programmed cell death ligand 1. Eno J. Immunotherapy Through the Years. *J Adv Pract Oncol.* 2017;8(7):747-753.

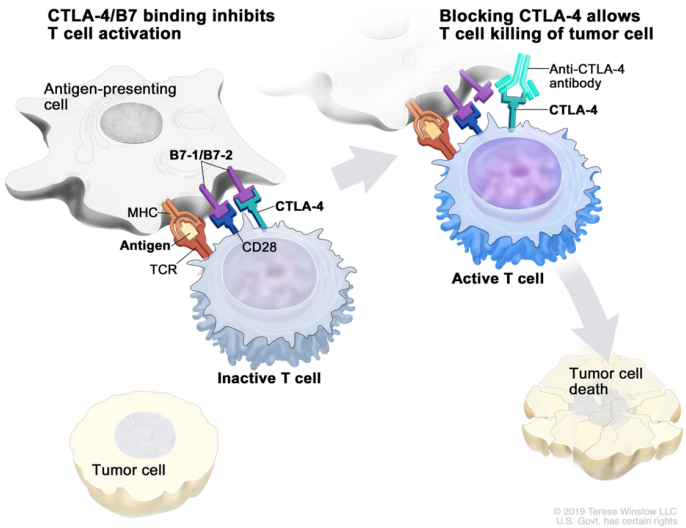

Figure 2. Mechanism of action of CTLA-4 inhibitors. Tumor cells develop B7-1/B7-2 to bind with CTLA4 on T-cells, which prevents T-cells from destroying the tumor cells (panel left). By blocking the ability of B7-1/B7-2 to bind to CTLA-4 with a CTLA-4 inhibitor, T-cells are then able to kill the tumor cells (panel right). CTLA-4 = cytotoxic T-lymphocyte-associated antigen 4. Eno J. Immunotherapy Through the Years. *J Adv Pract Oncol*. 2017;8(7):747-753.

2.3 Immunovirotherapy of melanoma

Melanoma is one best target for cancer immunovirotherapy. The first viral immunotherapeutic agent used in clinical settings was T-VEC that officially inaugurated the era of oncolytic virotherapy. T-VEC is the first FDA-approved oncolytic herpesvirus, genetically modified to selectively replicate within tumor cells and to increase tumor antigen presentation by dendritic cells (DCs) through granulocyte-macrophage colony-stimulating factor (GM-CSF) transgene expression (26).

T-VEC has been engineered to avoid the development of fever blisters by deleting the neurovirulence gene, infected cell protein 34.5 (ICP34.5). OPTiM, a randomized phase III trial (clinical trial identifier NCT00769704) that compared T-VEC and GM-CSF in patients with unresectable stage IIIB/C/IV melanoma reported that T-VEC improved longer-term efficacy versus GM-CSF alone (27).

Besides T-VEC, other types of OVs represent a promising strategy for the melanoma treatment and are involved in ongoing clinical trials such as oncolytic adenovirus ONCOS-102 (formerly named CGTG-102) (28) and parvovirus CVA21 (Cavatak) (29). ONCOS-102 (Ad5/3-.24-GM-CSF) is an engineered oncolytic adenovirus (Ad5/3) that expresses granulocyte-macrophage colony-stimulating factor (GM-CSF, 28). Its chimeric 5/3 capsid contains the fiber knob derived from Ad serotype 3, so infection can occur through binding of the desmoglein-2 receptor, which is often expressed on tumor cells (30, 31). Selective replication in tumor cells is provided by 24 bp deletion in the Rb binding site of the E1A gene restricting its replication to cells with p16-Rb pathway defects, such as most cancers (32). The local production of GM-CSF by ONCOS-102 ensures local concentration but minimizes systemic exposure and toxicity associated with GM-CSF. As reported by Bramante et al. nine patients received ONCOS-102 treatment for refractory melanoma had an extended survival of greater than 2,149 days and 559 days post treatment (30).

Coxsackievirus A21 (CVA21) is an emerging oncolytic virus may could have practical clinical application hereafter, although researchers are still establishing the capabilities of this virus against several malignancy**.** CVA21 infection is characterized by its interaction with the intercellular adhesion molecule-1 (ICAM-1, also termed CD54), which acts as the primary receptor for attachment and internalization, and decay-accelerating factor (DAF or CD55) a coreceptor acting as a secondary point of virus attachment (33).

Because melanoma is a malignancy with marked overexpression of ICAM-1 and DAF compared to normal cells (34), with lesions amenable to injection, studies of CVA21 in

melanoma are the most advanced, and may come to be regarded the best reliable for the evaluation of the efficacy of CVA21. The characteristic upregulation of ICAM-1 in melanoma is well established; indeed, it has been considered a clinically relevant marker of prognosis (35). In addition, a role for ICAM-1 in the generation of metastases has been suggested, as it facilitates cell-cell interactions between malignant melanocytes and circulating lymphocytes and spread of the disease (36). In the last years many clinical trials were conducted in which the oncolytic viral agent was combined with ICIs such as Pembrolizumab (NCT02565992) and Ipilimumab (NCT03408587) in patients with advanced melanoma. Then OVs due to their ability to selectively infect and replicate in tumor cells, as well as their capacity of attracting activated immune cells into the immunosuppressive tumor microenvironment, remain an appealing platform for cancer immunotherapy and in particular for combined strategies with ICIs.

Different OVs kill tumor cells by triggering different cell death pathways with diverse degrees of immunogenicity. OVs have been demonstrated to stimulate the immune system by infecting a tumor cell to induce immunogenic cell death (ICD), which triggers an inflammatory reaction. This particular form of apoptosis results in the release of immune stimulatory agents, which activate innate and direct adaptive immune responses against cancer cells by the release of pathogen-associated molecular patterns (PAMPS), tumor-associated antigens (TAAs), and danger-associated molecular patterns (DAMPS) from lysed tumor cells (37). Then OVs can recruit and activate tumor-infiltrating immune cells by releasing a large amount of tumor antigens and secreting cytokines (38).

Therefore, OV can be used as an in situ antigen-agnostic cancer vaccine within the TME (39). This can rapidly trigger acute innate immune responses consisting of dendritic cells, macrophages, and NK cells. These cells can further destroy OV-infected tumor cells and secrete pro-inflammatory cytokines (39). Moreover, these innate immune cells uptake viral and tumor antigens and present them for T-cell activation. Finally, activated T-cells proliferate and accumulate within the TME and exert their effect against cancer cells. In addition, T-cell-mediated adaptive immunity plays a crucial role in durable cancer control of distant tumor cells beyond the locoregional site of virus injection.

Then OVs treatment can remodel cold tumor in hot tumor by enhancing the tumor immunogenicity and intratumoral T-cell infiltration (39-41).

2.4 Current limitations of oncolytic adenovirus for cancer treatment

As previously descripted, OVs induce anti-tumor immunity through multiple mechanisms and represent an ideal platform for combination immunotherapy such as ICIs, even though there are still some barriers of oncolytic virotherapy to overcome in order to optimize OV-based immunotherapy (42). The first regards the choice of viral species considering that every virus has different biological characteristics such as genetic materials, pathogenicity size and shape. For instance, virus size is a crucial parameter since smaller viruses infiltrate and spread more easily within tumors, while larger viruses have larger genomes allowing a greater number of therapeutic genes to be inserted. Furthermore, DNA viruses must enter the nuclei of target cells to replicate whereas RNA viruses can replicate within the cytoplasm. Thus, the tumor specificity of DNA viruses depends on interactions between nuclear transcription factors (NTFs) and viral promoter/enhancer elements, although RNA viruses are not under the control of NTFs (43). Then, RNA viruses exert anti-tumor effects faster and are less selective with regards to tumors compared to DNA viruses. The presence of a viral capsid is also an important factor in OVs development because enveloped viruses are less oncolytic and can be more easily cleared by the host immune system (42).

A second barrier is represented by the route of administration. OVs can be delivered locally (mainly intratumorally) or systemically (mainly intravenously). Intratumoral injection is preferred because maximizes OVs concentration in target tumor lesions while minimizing systemic toxicity (42,44). The limits of this method consists in the impossibility to treat inaccessible or multifocal tumors; furthermore, treatment efficacy can vary depending on operator skill (44). Conversely, systemic administration is minimally invasive and highly reproducible, covering both primary and metastatic tumors. However, viral particles can be cleared rapidly by the host immune system, including neutralizing antibodies. To avoid this issue, envelope modification and the development of novel delivery systems using myeloid-derived suppressor cells (MDSCs) as viral carriers have been explored to deliver OVs to tumor sites (44).

To maximize the therapeutic efficacy of OV treatment novel delivery platforms have been developed such as nanoparticles, liposomes, polyethylene glycol (PEG) for delivery of OVs in the systemic circulation to the local TME (45). A promising carrier system to effectively deliver viruses to tumor cells is the magnetic drug targeted system (46). Hence, discovering the optimal route of administration and enhancing the homing of OVs to tumor sites is pivotal for improving anti-tumor efficacy.

The levels of intratumoral OV infiltration and diffusion are critical to exert therapeutic efficacy. The TME includes proteins of the extracellular matrix (ECM) that serves as a physical barrier to intratumoral OV infiltration and diffusion (44,47). In order to overcome this barrier, new OVs have been engineered to express enzymes capable to ECM degradation, to enhance anti-tumor activity (48,49).

As previously mentioned, the main advantage of using oncolytic viruses (OVs) is their ability to modulate the TME rendering it less immunosuppressive (50). OVs can preferentially infect and kill cancer cells as result of the inhibition of the dysfunctional Type I IFNs signaling (51); however, their main ability consists in triggering a response from the immune system, impaired by the hostile and highly immunosuppressive environment of the tumor milieu. Cancer cells can hinder immune control of tumors by secreting cytokines, such as interleukin-10 (IL-10), chemokines, such as chemokine C-X-C motif ligand 12 (CXCL12), growth factors, such as transforming growth factor beta (TGF-β), arginase-1, matrix remodeling factors, such as collagen, fibronectin, and fibrin, and other soluble factors, such as adenosine, into the TME (52,53), reducing the amplitude of OV-induced anti-cancer immune responses (54,55). To counteract the immunosuppressive TME, different OVs have been modified to express immune-activating cytokines or chemokines ot T-cell costimulatory molecules to stimulate effector function of T- cell within TME thereby triggering immunostimulatory signals within the TME (44,52,53,57,56,) and enhancing anti-tumor immunity (58-59).

Despite the multipower of OVs, all that glitters is not gold because the antitumor-immunity generated by OVs is hampered by the classical anti-viral response from normal cells (38,60). In case of repeated OV administration, viral replication can be suppressed by anti-viral immunity that in turn promotes viral clearance and shrinks anti-tumor activity in immunocompetent patients (50,61-62) as shown for T-VEC (61) and Vaccinia virus H3L envelope (63). Despite the antiviral immunity-related negative effects, some consider that it could be beneficial for anti-tumor immunity

because anti-viral immunity can recruit anti-tumor immune cells into the tumor milieu and reverse its immunosuppressive environment (42). Thus, finding the balance between anti-viral and OV-induced anti-tumoral immunity may be a crucial factor to maximize the efficacy of OV therapy.

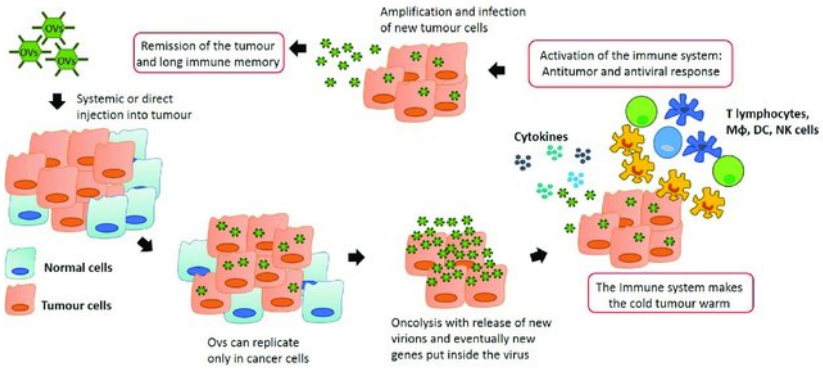

Figure 3. Anti-tumor immunity by oncolytic virus (OV) therapy. OVs can be modified in order to replicate only in transformed cells. This process stimulates the immune system which is recruited into the tumor, tipping the neoplastic mass from an immuno-suppressive environment to an inflammatory site. Marelli, G., Howells, A., Lemoine, N. R., & Wang, Y. (2018). Oncolytic Viral Therapy and the Immune System: A Double-Edged Sword Against Cancer. *Frontiers in immunology*, *9*, 866.

2.5 The role of intestinal microbiota in cancer

The community of microorganisms, including bacteria, archaea, viruses, and yeast, living in a specific environment is the perfect definition of a microbiota. On the other hand, a microbiome is the entire collection of all the genomic elements of a specific microbiota. Metagenomics is the field of molecular research that studies the complexity of microbiomes. Gut microbiome, which hosts up to 1,000 bacterial species that encode about 5 million genes, exert many of the functions required for host physiology and survival. Human gut microbiome is not a static system and changes with host development. The complexity and dynamic nature of this system leads variation in the density and composition of the microbiome along longitudinal and transverse gradients (64). As such, distinct micro-ecosystems reside in different locations of the gut, including the lumen, the mucosa and intestinal crypts (65).

Taxonomically, bacteria are classified according to phyla, classes, orders, families, genera, and species. Only a few phyla are represented, accounting for more than 160 species (66). Gut microbiota is composed primarily of the phyla Firmicutes, Bacteroidetes, Actinobacteria, Proteobacteria, Fusobacteria, and Verrucomicrobia; in particular the two phyla Firmicutes and Bacteroidetes represent 90% of gut microbiota (67). More than 200 different genera such as *Lactobacillus*, *Bacillus*, *Clostridium*, *Enterococcus*, and *Ruminicoccus* represent about 95% of the Firmicutes phyla. Bacteroidetes consists of predominant genera, such as *Bacteroides* and *Prevotella*, whereas the Actinobacteria phylum is proportionally less abundant and mainly represented by the *Bifidobacterium* genus (67,68).

The microbiota can influence human health by preventing growth of pathogens, producing beneficial microbial products and metabolizing nutrients and toxins. Although most research has focused on the relationship between the intestinal microbiota and obesity, there is growing awareness that the microbiome influences tumor progression, in part through inflammatory and immune circuits. The relationship between the gut microbiome and cancer is multi-factorial and most likely bidirectional; in fact, cancer-associated perturbations in the microbiome may occur as a result of the disease but may also contribute to cancer progression (69).

Tumorigenesis can affect the microbiome through several mechanisms. Failure of immunosurveillance promotes development and progression of malignancies; this defects in immune-system is often associated with systemic immunosuppressive effects, which can

alter the balanced ecosystem of microbiota. In addition, cancer can affect host metabolism, and this also can perturb the gut microbiome (69). Conversely, alterations in the microbiota may contribute to carcinogenesis at multiple levels (70).

Scientists have proposed various mechanisms: first, by direct oncogenic effects of microorganisms or their products. Second, by microbiota-mediated alterations in circulating metabolites that affect tumor progression. Third, by inducing pro-inflammatory and immunosuppressive effects that may subvert anticancer immunosurveillance. Thus, the microbiota can contribute to the development of malignant disease through several mechanisms.

Thanks to Next-Generation Sequencing (NGS) of 16S rRNA bacterial gene, we can explore human microbiome, focusing on the gut microbial profile in cancer patients versus healthy control, identifying bacteria genera and species with increased gut colonization during the carcinogenesis and conversely those that decrease. In addition, multiple associations have been reported between the abundance of specific bacterial phyla and species in distinct cancer-associated locations (71-73).

The gut microbiota of the colorectal cancer (CRC) patients has been deeply investigated, they were enriched in *Bacteroides fragilis*, *Enterococcus*, *Escherichia/Shigella*, *Klebsiella*, *Streptococcus* and *Peptostreptococcus* and were depressed in *Roseburia* and other butyrate-producing bacteria of the family Lachnospiraceae (74). Healthy volunteers showed a gut microbiota enriched in *Bacteroides vulgatus* and *Bacteroides uniformis*. Specific gut microbiota variances, such as a reduction of butyrate producers and an increase in opportunistic pathogens, represent a key structural imbalance of gut microbiota in CRC patients. Data published by Shen et al. (75) showed a higher abundance of Proteobacteria and a lower abundance of Bacteroidetes in CRC cases compared to controls. Genomic analysis identified an association of Fusobacterium spp. with colorectal cancer; therefore, Fusobacterium spp. may contribute to tumorigenesis by an inflammatory-mediated mechanism (76). However, the precise role of Fusobacteria in colorectal carcinoma pathogenesis requires further investigation.

All these findings reveal alterations in CRC microbiota that may contribute to the etiology of colorectal cancer. Additional evidences may lead to strategies to manipulate microbiota to prevent colorectal cancer as well as to identify individuals at high risk (75). So far, several data have been published on the relationship between bacteria and other type of tumors, but the majority of the studies have a single patient cohort, and therefore cannot be used

to make general assumptions on the relationship between bacteria and cancer development, progression and therapeutic responses.

2.6 Gut microbiota in cancer Immune response and immunotherapy

As mentioned in the previous paragraph, many researchers observed associations between certain microbiome profiles and the development and progression of cancer**.** In particular, some interventional approaches change the gut microbiome composition in cancer patients and in turn may affect oncogenesis. Long-term use of antibiotics, fecal microbiota transplantation (FMT), nutritional interventions, such as caloric restrictions and prebiotic and/or probiotic formulations interventions, may cause permanent changes in the microbiome. These regimens can make a positive selection of beneficial species or negative selection of harmful species in the microbiota (69).

A study published in 2016, suggested that antibiotic-induced changes in microbiome may affect the metabolism of sex hormones, such as estrogen, thereby influencing the risk of breast cancer (77). In a previous evaluation in mouse model, Viaud et al. observed that vancomycin negatively affects the induction of cyclophosphamide-triggered anti-cancer immune responses (78). Conversely Vetizou et al. provided strong evidence in support of the immunomodulatory activity exerted by gut microbiota, confirmed by lost therapeutic activity of CTLA-4 against sarcoma in mice housed under specific pathogen-free (SPF) conditions treated with multiple broad-spectrum antibiotics. Specifically, oral treatment with the antibiotic vancomycin, which mostly eliminates gram-positive bacteria, improves the outcome of anti-CTLA-4 therapy, likely by inducing an expansion of bacteria of the order Bacteroidales, at the expense of members of the Clostridiales. The expanded population of immunogenic gram-negative bacteria triggers type 1 T helper (Th1) immune responses, which increases the antitumor efficacy of CTLA-4 blockade (79). The effects of antibiotic modulation of the microbiome during cancer treatments are complex and all the data actually available suggests that antibiotic-mediated effects are context dependent and can be either beneficial or harmful.

Fecal microbiota transplantation (FMT) is a promising approach to restore gut microbiota dysbiosis and involves exchanging of gut bacterial content between individuals. Compared with other manipulations of the microbiome, FMT induces a long-term reset the microbiome restoring a new balanced ecosystem. In mouse models, FMT may reduce

colorectal carcinogenesis (80-81); however, its remains unclear whether FMT could reduce the process of carcinogenesis and tumor progression in humans.

Caloric restriction is the most potent and reliable physiological intervention for increasing life expectancy and reducing the incidence of cancer in mouse and non-human primates (82-83). Nutrient deprivation indices a reduction in the Firmicutes/Bacteroidetes ratio, as well as the enrichment of *Akkermansia muciniphila* in humans (84-85).

Starvation induces a rapid fucosylation of the intestinal epithelium, thus providing nutrients for commensal bacteria and reducing the probability of pathogenic invasion, in mice model (86). Some studies illustrated the links between caloric restriction and cancer indicating that cyclic short-term fasting improves anticancer immunosurveillance in mice, through the induction of autophagy in malignant cells and by systemic immunostimulation (87,88). The question to answer is whether starvation-induced changes in the composition or function of the microbiome contribute to these beneficial effects.

Prebiotics induce growth or activity of so called “beneficial bacteria” that are able to promote a condition of healthy gut (80). Non-digestible polysaccharides, metabolized by bacteria to short-chain fatty acids (SCFAs), increase the abundance of Bifidobacterium spp. that reportedly reduce tumor growth, notably in the context of programmed cell death 1 (PD1) blockade (89).

Probiotics are live microorganisms that are intended to have health benefits because reinforce natural defence, protect against gastrointestinal disorders and pathogens, and enhance innate and adaptive immunity. Several probiotics may mediate immunomodulatory (90). Lactobacillus spp., which belong to the group of lactic acid bacteria, are prominent probiotic organisms (91). Numerous reports have shown that different isolates of *Lactobacillus casei*, *Lactobacillus plantarum*, *Lactobacillus rhamnosus* GG, and *Lactobacillus acidophilu*s may mediate anticancer effects through various mechanisms, such as natural killer (NK) cell activation and DCs maturation (90,92,93).

Abundant in some milk products and naturally found in the colon, members of Bifidobacteriales, have been associated with immune health in humans. Members of the Bifidobacteriales were abundant in mice that exhibited reduced growth of melanomas and improved Cytotoxic T-lymphocytes (CTL)-mediated immunosurveillance (89). Supplementation with Bifidobacterium breve or Bifidobacterium longum into Bifidobacteriales-free mice was sufficient to reduce melanoma growth and restore anti-melanoma CTL responses. Furthermore, *B. breve* and *B. longum* increased DC maturation, enabling DC priming of tumor-specific CTLs. In mice that carried *B. breve* or *B. longum*, CTL-

infiltrated tumors responded better to PD-L1 treatment compared to tumors of sterile or Bifidobacteriales-free mice (89).

Altogether these data confirmed that gut microbiome has a key role in modulating immune responses of different categories of cancer treatment, in particular of ICIs, in mice model and in patients, supporting that anti-cancer therapies can influence the gut microbiome, which, in turn, affects treatment outcome and could be responsible of the variability observed in clinical outcomes (79,89,94-96).

RESEARCH AIM

Commentato [LT1]: Correction 1

Despite the role of the gut microbiome in modulating ICIs efficacy has been widely considered in many types of cancers, the role of the gut microbiome in modulating oncolytic immunotherapy in solid tumors, was never investigated. In addition, considering that OVs are an optimum candidate to combine with ICIs, whose efficacy is gut microbiome-mediated, we decided to focus on possible relationship between gut microbiota and viroimmunotherapy. We investigated whether gut microbiota could affect the antitumoral activity of oncolytic adenoviral vaccine. First, we planned to investigate whether microbiota depletion, after antibiotic treatment, could influence the response to oncolytic adenovirus therapy. Secondly we evaluated the possible synergistic antitumor activity exerted by *Bifidobacterium spp*. probiotic combined with Ad-CpG; then we studied the fecal microbial profile of mouse model of melanoma.

3.MATERIALS AND METHODS

3.1 Cell lines and reagents

A549 cells, a human cell line isolated from lung adenocarcinoma, were grown using alpha-MEM culture medium supplemented with 10% FBS, 1% P/S and 1% L-Glu. Upon reaching 80% of confluence, the cells were split, counted and seeded at a density of $2.6x10^6$ cells in 150 mm dishes .B16.OVA, a mouse melanoma cell line expressing chicken OVA and derived from C57BL/6J, was kindly provided by Prof. Vincenzo Cerullo. Cell line was cultured according to ATCC recommendations in RPMI 1640 medium. Medium was supplemented with 10% heat-inactivated fetal bovine serum (FBS, Gibco), penicillin (50 U/mL), streptomycin (500 µg /ml), and glutamine (4 mmol/L). 1% of Geneticine (GIBCO) was added to the cell culture od B16.OVA cells. Both cell lines were cultured in an incubator under humidified atmosphere at 37 ° C of 5% CO_2.

3.2 Virus amplification and purification

Ad5D24-CpG is an oncolytic adenovirus bearing a CpG-enriched genome in the E3 gene. Ad5D24-CpG was generated recombining a CpG-rich shuttle plasmid (pTHSN-CpG1) with a plasmid containing the 24 adenovirus backbone by Cerullo et al (97). It was amplified to perform all experiments described in the section results. The amplification of the virus was performed by infecting A549 cells at 70-80% confluence with the oncolytic adenovirus Ad5D24-CpG at a MOI (multiplicity of infection) equal to 10 pfu / cell. After 72h, upon reaching the cytopathic effect (CPE), the cell lysate was collected and stored at -80 ° C.
Subsequently, to induce cell lysis, the sample was subjected to three freeze-thaw cycles and then centrifuged at 4,000 rpm for 25 min at 25 ° C. The supernatant containing the virus was collected and purified from the lysate by a first step in an ultracentrifuge at 27,000 rpm for 1-2h at 4 ° C on a CsCl gradient. The band containing the oncolytic adenovirus was subjected to a further ultracentrifugation step under the same conditions described above for a time exceeding 18h. Once isolated, the sample was dialyzed by placing it in TM solution (10 mM Tris-HCl pH 8.0, 2 mM MgCl2) for 2h under stirring at 4 °

C. After 2h, the dialysis cassette was transferred to the Freezing solution (10 mM Tris-HCl pH 8.0, 2 mM MgCl2, 4% sucrose) overnight at 4 ° C under stirring. The virus was collected, aliquoted and stored at -80 ° C. Ad5D24-CpG was titrated by spectrophotometric reading, obtaining a titer of $4.4x10^{11}$ vp / ml.

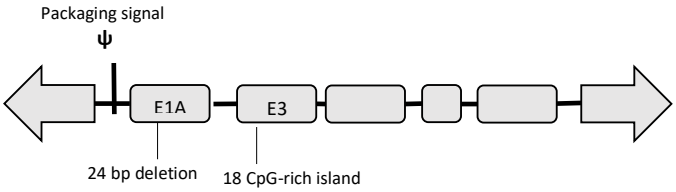

Figure 4: Schematic representation of Ad5D24-CpG. This virus bears a 24 bp deletion in E1A gene for selective replication in cancer cells and 18 CpG-rich islands to increase Toll-like receptor 9 (TLR9) stimulation.

3.3 Tumor cell lysis assays

Tumor cell lysis was determined through the quantitative analysis of Lactate dehydrogenase (LDH) using an LDH Detection Kit (Cyquant, Invitrogen), according to the manufacturer's instructions. The dosage of LDH activity was performed on the cell cultures supernatants collected 48-hours after of co-culture assay, by spectrophotometric reading at 490nm. The B16-OVA were plated and incubated for 16 hours at 37 ° C, and successively pre-immunized murine splenocytes were added. After 48 hours of incubation at 37 °C, images of each experimental point, before and after the removal of the murine splenocytes (Figure 14, panel C) were captured by a phase contrast microscopy.

3.4 Animal experiments and ethical permits

All animal experiments were reviewed and approved by the Experimental Animal Committee of CEINGE Biotecnologie Avanzate and the Provincial Government of Italy (number D5A89.41). Female C57BL/6J 6-8 weeks old were obtained from Charles Rivers and used as syngeneic mouse melanoma model. 3.5 x 10^5 B16.OVA cells were engrafted subcutaneously in right or both flanks of animals (only in the experiment shown in Figure 11).Mice were fed with diet standard (Muscendola) and housed in biosafety levels 2 (BSL-2) room in animal facility at CEINGE Biotecnologie Avanzate. Drinking water was sterilized in an autoclave and changed every two days. In the present study we collected the following biological samples from all enrolled animals: spleen and tumor samples for flow cytometry analyses and feces samples. Spleen and tumor samples were triturated into single cells in sterile freezing medium with 90 % FBS and 10% DMSO medium, then filtered by cell strainer 70 µm and stored at -80°C. Feces samples were immediately cooled in dry ice and stored at −80 ◦C until the DNA isolation for microbiome analysis.

3.5 Tumor implantation and tumor growth measurement

At day 0, 3.5 × 10^5 B16.OVA cells diluted in 200 µl of PBS were injected subcutaneously into the right flank or in both of each mouse. Tumors were measured with an electronic digital caliper every two days , starting from day 7 post tumor injection. Tumor volume was calculated as length × width × height (in mm^3). Mice were sacrificed when the tumor volume was greater than 1800 mm3 or when they were in poor condition and expected to die shortly. Tumors and spleens were collected and used for further experiments. In another experiment (Figure 2), mice survival has been followed until the end.

Virus injection

Before each virus injection, mice were anesthetized in an isoflurane chamber. Then, they were injected intratumorally with 10^9 vp Ad5D24CpGat day 9, 11 and 13 after tumor injection. The protocol schedule of tumor and Ad-CpG injection is shown in Figure 7, panel A.

3.6 Bifidobacterium and antibiotic treatment.

A cocktail of lyophilized Bifidobacterium species (*B. bifidum, B. longum, B. lactis and B. breve*- Seeking Health) was resuspended in PBS at $5x10^9$ CFU/ml (Figure 5). Each mouse was given 200µl of Bifidobacterium ($1x10^9$ CFU/mouse) by oral gavage ten days before the cancer cell inoculation (Day 0) and at day 9, 11, 13, 15, 17 and 19 day after the cancer inoculation. Mice were treated with vancomycin two weeks before tumor cells inoculation and continued until the first injection of Ad-CpG. Vancomycin (0.25mg/ml Mylan) was administered by oral gavage every two days (Figure 6).

Figure 5: Label of Bifidobacterium cocktail mix supplied by Seeking Health and used in the experiment in vivo. It contains 4+ billion CFUs of *Bifidobacterium bifidum*, 3+ billion CFUs of *Bifidobacterium longum*, 2+ billion CFUs of *Bifidobacterium lactis* and 1+ billion CFUs of *Bifidobacterium breve*

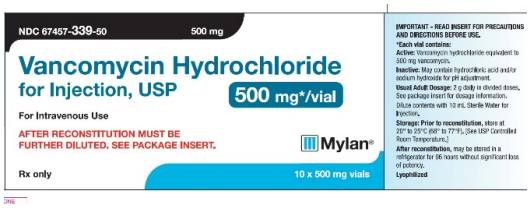

Figure 6: Vancomycin Mylan 500 mg/vial, powder for solution for infusion.

3.7 Isolation of immune cells from mice spleen and tumor

After the collection of spleen from mice, spleen and tumor were kept into sterile RPMI 1640 medium, supplemented with 90% heat-inactivated fetal bovine serum (FBS, Gibco)

and transferred into a 70 µm cell strainer fitted on a 50 mL tube. Then spleen/tumor was gently cut it into small pieces using a 5 mL syringe plunger and pressed through the cell strainer. Once collected the cells, media up to 25-30 mL was added and were centrifuged at 2000 rpm, 10 min, at +4°C. The cells collected by spleen were treated with 5 mL ACK lysis buffer, and incubate on ice for 5 min to lyse red blood cells. Both cells, collected from spleen and tumor, were centrifuged at 2000 rpm, 10 min, at +4°C and filtered through a new 70 µm cell strainer, to remove dead cell clumps and other debris. Some cells were used directly on cell assays, and other were frozen in a medium supplemented with 90% of FBS and 10%of DMSO.

3.8 Flow Cytometry analysis

Surface and intracellular staining were performed using the following antibodies: CD3 PerCP-Cy5.5 (eBioscience, San Diego, California); CD8 FITC (eBioscience); CD4 PeCy7 (eBioscience); CD45R/B220 APC (Biolegend, San Diego, California); anti-mouse CD45 APC-Cy7 (Sony Biotechnology, San Jose, California); anti-mouse IFN-γ PE (Sony Biotechnology); anti-mouse Foxp3 PE (eBioscience). Cell stimulation cocktail (eBioscience); Brefeldin A (eBioscience). Cells were initially stained with surface markers (CD3, CD8, CD4, CD45R/B220 and CD45) and then stained for FOXP3 (Fox-P3/Trascription Factor Staining Buffer Set, eBioscience) using a protocol for nuclear detection, according to manufacturers' instructions. T-cells were stimulated to produce IFN-g in vitro using Cell stimulation cocktail (eBioscience) and its secretion was blocked using protein transport inhibitors (Brefeldin A Solution (eBioscience). Successively cells were stained with surface markers (CD3, CD8, CD4, CD45R/B220 and CD45) and then stained for IFN-g using a protocol for cytoplasmic detection, according to manufacturers' instructions. All stained cells were acquired by FACS Canto II cytometer (BD Biosciences Franklin Lakes, NJ) and analyzed with FACS Diva software (BD Biosciences).

3.9 Microbial Sequencing-16S rRNA

Five fecal samples were collected from every group (n=5 mice/group) at different timepoints: before the inoculation of B16.OVA cells (Day-10), when tumor has reached a diameter of 5mm and before to start treatment (Day 0), the day before the last feeding

integration with the Bifidobacterium mix (Day 18), and at the end of the experiment in vivo (Day 20). DNA was extracted from fecal samples using QIAamp DNA mini kit (Qiagen, Venlo, The Netherlands). All extractions were performed in a pre-PCR designated room. To deeply investigate the microbiome composition, we used a multiplexed 16S rDNA amplicon-based approach coupled with the NGS system MiSeq (Illumina, San Diego, CA, USA). In particular, 500 bp amplicons, spanning the V4-V6 hyper-variable regions of the 16S rRNA gene, were obtained. Each sample was individually amplified and purified (Agencourt AMPure XT beads, Beckman Coulter, Brea, CA, USA). Primers used in the first round of PCR contained the overhang sequences with Illumina adapters (in bold): forward primer, 5'-**TCGTCGGCAGCGTCAGATGTGTATAAGAGACAG**CCAGCAGCCGCGGTAA -3'; reverse primer, 5'- **GTCTCGTGGGCTCGGAGATGTGTATAAGAGACAG**GGGTTGCGCTCGTTGC - 3'. PCR conditions were 95°C for 10 min; 30 cycles of 95°C for 30 s, 59°C for 30 s, 72°C for 1 min; 72 ◦C for 7 min and 4°C to the end. A second round of PCR was used to add the Illumina index to the amplicons for the library preparation according to the Nextera XT protocol (Illumina). PCR conditions were 72°C for 3 min; 95°C for 30 sec; 12 cycles of 95°C for 10 s, 55°C for 30 s, and 72°C for 30 s; 72°C for 5 min and 10°C to the end. After appropriate quality assessment (TapeStation, Agilent Technologies, Santa Clara, CA, USA), the amplification products from different DNA samples were pooled in equimolar ratios. The obtained multiple amplicon libraries were quality assessed (TapeStation, Agilent Technologies) and quantified (Qubit dsDNA BR assay, Thermo Fisher, Waltham, MA, USA), according to the manufacturer's instructions, in order to obtain a pool of equimolar libraries, so ensuring a normalization across the different samples sequenced in the same run. All libraries were sequenced with the Illumina MiSeq System, PE 300x2 protocol, according to the specifications of the manufacturer.

3.10 Microbiome Data Processing

Quality of microbial sequences was controlled using MultiQC v1.5 [1]. Reads adapters and low-quality reads/ends were removed using Trimmomatic v0.38 . To analyze the taxonomic composition of samples, DADA2 v. 1.15.0 (98) and Phyloseq 1.28.0 (99) R packages were used (R version 3.6.1). A scarce overlapping between paired-end reads was observed. We chose to analyze only the forward reads to have a more reliable alignment. Before aligning reads, the forward primer was trimmed out from reads and reads were filtered according to the following parameters: maxEE=2; minLen = 50; maxN=0; truncQ=2.

After chimeric sequences removal, taxonomy was assigned to ASVs (Amplicon Sequence Variants) by using the SILVA reference database v.128, formatted for being used by DADA2 software and available at the link https://zenodo.org/record/824551#.XmIcO5NKhuU.

The phylogenetic tree was constructed by performing a multiple-alignment using the DECIPHER 2.12.0 R package (100). The phangorn 2.5.5 R package (101) was then used to first construct a neighbor-joining tree, and then fit a GTR+G+I (Generalized time-reversible with Gamma rate variation) maximum likelihood tree using the neighbor-joining tree as a starting point.

Statistical analyses of the dataset were carried out through combining all the data (cleaned ASVs, taxa assignment, phylogenetic tree, and metadata) into a phyloseq object.

The α- and β-diversity were computed on the counts normalized with the respect to the total and the ANOSIM tests were performed. Wilcoxon rank-sum test (Mann-Whitney) was applied to test significance in terms of richness measured by the several α- diversity distances.

The significance of differential abundance among groups at different taxonomic levels was assessed by Kruskal-Wallis Rank Sum Test in R environment (102). The pairwise comparison was then performed by Dunn's test (103), through FSA 0.8.27 package, on the significant Kruskal-Wallis tests and the p-value corrected for multiple comparisons by the Benjamini-Hochberg adjustment method.

4.RESULTS

4.1 Gut microbiota affects the response to an oncolytic adenovirus in a syngeneic mouse model of melanoma

The observation that anticancer immunotherapy with CTLA-4 blockade is affected by gut microbiota composition (79) prompted us to investigate whether also oncolytic virotherapy efficacy could be influenced by intestinal microbes.

At first, we planned to investigate whether microbiota depletion and unbalance after antibiotic treatment could influence the response to the treatment with the oncolytic adenovirus Ad5D24-CpG (Ad-CpG). At this aim, we treated a group of mice with vancomycin two weeks before the tumor cells inoculation and until the first intratumoral administration of Ad-CpG, as indicated in experimental design (Figure 7, panel A). The group of mice treated with vancomycin and Ad-CpG had a faster tumor growth compared to the group treated with Ad-CpG alone (Figure 7, panel B); interestingly, tumor growth in the group of mice that received vancomycin and Ad-CpG was comparable to what observed in mice treated with vancomycin alone. Therefore, vancomycin treatment seems to abrogate the efficacy of onco-virotherapy. The Ad-CpG-treated tumors showed a significantly slower growth-kinetics as represented by the area under the curve analysis (AUC, Figure 7, panel C). Furthermore, the reduced response observed in mice treated with Ad-CpG combined with vancomycin can be well appreciated considering the single tumor growth curves for each mouse treated (20% responders, Figure 7, panel D). Vancomycin treatment reduced tumor growth compared to mock-treated mice; this observation is consistent with the current literature (104). In order to determine how vancomycin pre-treatment influences the immune response induced by Ad-CpG, we analyzed the phenotype of tumor-infiltrating lymphocytes (TILs) in tumors. Levels of both CD4+ and CD8+ T-cells were not affected by vancomycin pretreatment (Figure 8, panel A); however, the percentage of IFN-gamma-producing CD8+ T-cells was significantly lower in mice that received the combined treatment (Ad-CpG + vancomycin) compared to mice treated with only Ad-CpG (Figure 8, panel B). These data suggest that pre-treatment with antibiotic causes a reduction of the IFN-gamma-secreting CD8+ T-cells infiltrating the tumor blocking the efficacy of oncolytic virotherapy.

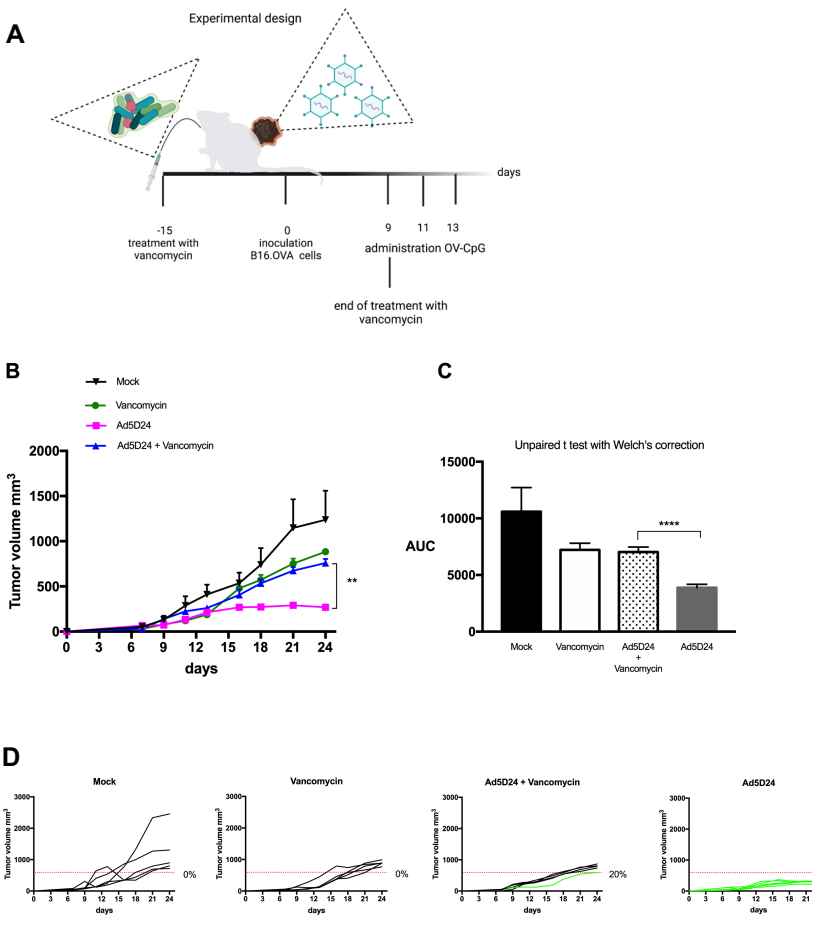
A
Experimental design
days
-15
treatment with
vancomycin
0
inoculation
B16.OVA cells
9
11
13
administration OV-CpG
end of treatment with
vancomycin
B
Mock
Vancomycin
Ad5D24
Ad5D24 + Vancomycin
Tumor volume mm3
2000
1500
1000
500
0
0
3
6
9
12
15
18
21
24
days
**
C
Unpaired t test with Welch's correction
AUC
15000
10000
5000
0
****
Mock
Vancomycin
Ad5D24
+
Vancomycin
Ad5D24
D
Mock
Vancomycin
Ad5D24 + Vancomycin
Ad5D24
Tumor volume mm3
days
0%
0%
20%

Figure 7. Perturbation of gut microbiome reduced the efficacy of oncolytic adenovirus in syngeneic mouse model of melanoma. A) Experimental design: antibiotic vancomycin was administered by oral gavage every two days, 15 days before tumor implantation. At day 0, $3x10^5$ B16.OVA cells were injected in the flank of female C57BL/6J mice (n=5 per group). Ad-CpG was administered intratumorally on days 9, 11 and 13. **B)** tumor-bearing mice (n=5 per group) were treated with saline solution (Mock), 100 µl of vancomycin (10mg/ml), $1x10^9$ vp/tumor of Ad-CpG and with a combination of Ad-CpG + vancomycin. Tumor size was measured at each time point for each mice; results are graphed as mean for each treatment groups ± SEM; statistical difference has been determined with 2way ANOVA (*p < 0.05, **p < 0.005). **C)** The area under the curves relative to the tumor growth of mice was calculated and plotted as the mean ± SEM. **D)** The single tumor growth curves for each tumor treated in every mouse and one graph for each group are reported (n = 5 animals per group). Responders are defined in percentage (displayed next to each graph) as mice that show an absolute volume lower than 594,1 mm^3. The tumors responder are represented by green curves and tumors non-responder are represented by black curves.

Commentato [LT2]: Correction 3

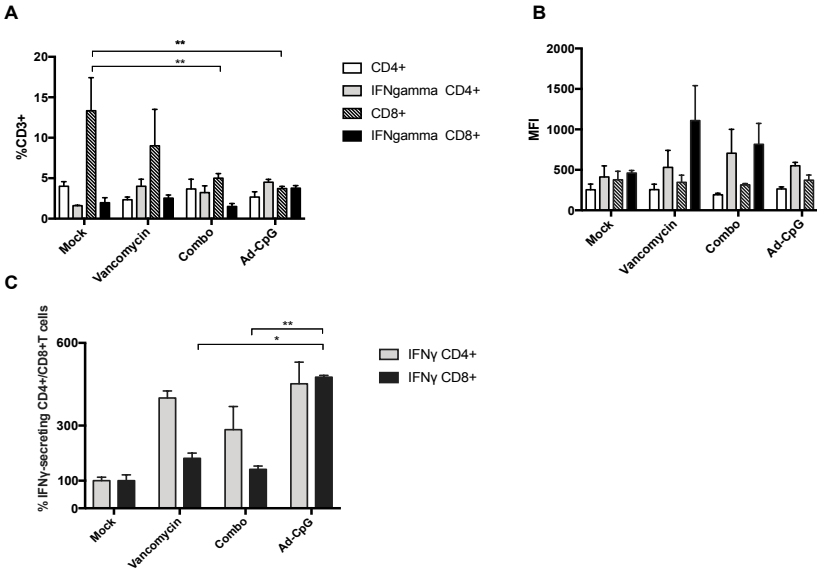
A
%CD3+
20
15
10
5
0
**
**
CD4+
IFNgamma CD4+
CD8+
IFNgamma CD8+
Mock
Vancomycin
Combo
Ad-CpG
B
MFI
2000
1500
1000
500
0
Mock
Vancomycin
Combo
Ad-CpG
C
% IFNγ-secreting CD4+/CD8+T cells
600
300
100
0
**
*
IFNγ CD4+
IFNγ CD8+
Mock
Vancomycin
Combo
Ad-CpG

Gating strategy

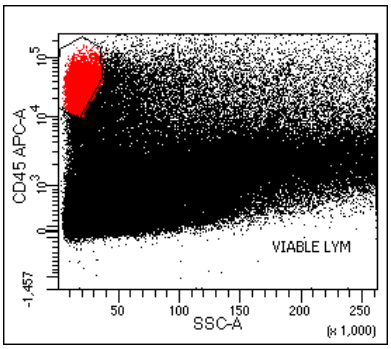

Viable lymphocytes (LYM)

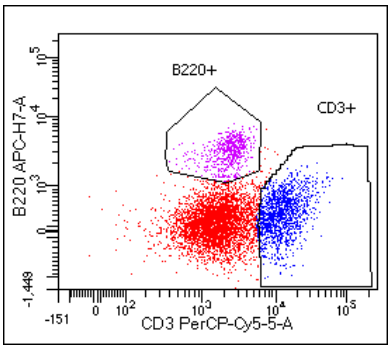

CD3+ T LYM

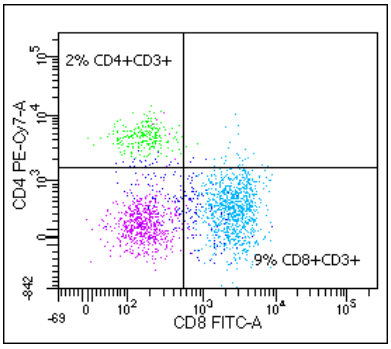

Vancomycin

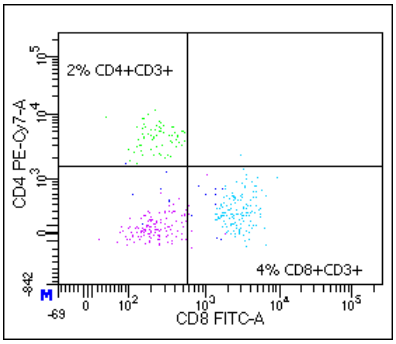

Ad-CpG

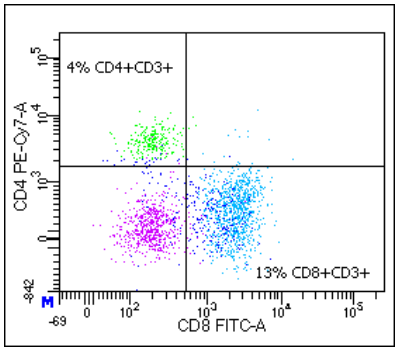

Mock

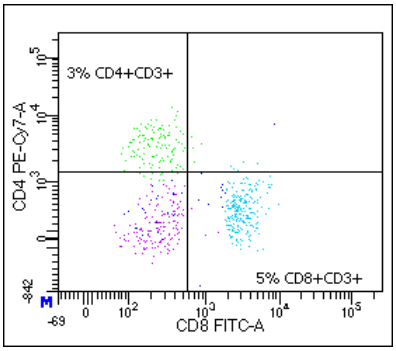

Combo

Figure 8. Evaluation of subsets of T-cell in tumor samples. A) Percentages of total CD3+ CD4+ T lymphocytes, IFN-γ CD4+ CD3+, CD3+ CD8+ T lymphocytes and IFN-γ CD8+ CD3+ T cells analyzed in the tumors. The statistical significance was evaluated by Two way ANOVA test using Tukey's multiple comparisons test and the asterisks indicate statistical significance (***p<0.001; **p<0.01; *p<0.05) compared to CD8+CD3+ of mock tumor. The vertical lines indicate the standard single error of the mean (SEM). **B)** Mean Fluorescent Intensity (MFI) of T cells represented in the plot A. The vertical lines indicate the standard single error of the mean (SEM). **C)** Percentages of IFN-γ+CD4+CD3+ and IFN-γ+CD8+CD3+ T cells calculated as ratio of IFNγ+CD4+CD3+/CD4+CD3+ and ratio IFNγ+CD8+CD3+/ CD8+CD3+ and normalized on ratio value of mock group. The statistical significance was evaluated by paired student's T-test and the asterisks indicate statistical significance (***p<0.001; **p<0.01; *p<0.05) compared to % IFNγ+CD8+ of Ad-CpG -treated tumor. The vertical lines indicate the standard single error of the mean (SEM). The panel below represents the quadrant gating strategy that has been used for all samples. The lymphocytes gate was obtained selecting CD45+ viable lymphocytes (red color population indicated as LYM, left panel) and then T lymphocytes CD3+ were gated on CD45+ lymphocytes (right panel). B220 was used to select B lymphocytes on CD45+ viable lymphocytes. For each treatment, we report the gate strategy of CD8+CD3+CD45+ and of CD4+CD3+CD45+ T lymphocytes.

Commentato [LT3]: Correction 4 and 5

4.2 Restoring gut microbiota balance revert the effect of vancomycin treatment on the efficacy of oncolytic adenovirus treatment

In order to confirm that the reduced efficacy of Ad-CpG was due to gut microbiota alterations, we cohoused a group mice treated with vancomycin and Ad-CpG (combined regimen) with a group of mice treated with Ad-CpG alone, as indicated in the experimental design (Figure 9, panel A). We compared subcutaneously B16.OVA melanoma growth in this group to a group of mice treated with Ad-CpG and vancomycin and kept isolated. We observed that cohousing significantly reduces differences in tumor growth between mice treated with combined regimen and mice treated with Ad-CpG alone, indicating that a positive perturbation and possibly a restoration of gut microbiota occurred (Figure 9, panel B). In addition, tumors of mice treated with combined regimen and cohoused showed a significantly slower growth kinetics compared to isolated mice as represented by the area under the curve analysis (AUC, Figure 9, panel C). In fact, complete response was observed in 100% of the cohoused mice treated with the combined regimen while it was observed in 67% of mice treated with the combined regimen kept isolated (Figure 9, panel D). When compared to mock-treated group of mice, overall survival of mice pre-treated with vancomycin was significantly improved by cohousing (median survival 40 days; Figure 9, panel E), compared to isolated mice (median survival 25 days; Figure 9, panel E). We then investigated the levels of IFN-gamma-producing CD4+ and CD8+ T-cells in tumors. Interestingly, IFN-gamma CD4+/CD4+ T-cells ratio in tumors treated with combined regimen and cohoused was 2.78 compared to a 0.34 ratio in tumors of isolated mice (Figure 10, panel A). Similarly, IFN-gamma CD8+/CD8+ T-cells ratio in tumors treated with combined regimen and cohoused was 0.51 compared to a 0.16 ratio in tumors of isolated mice (Figure 10, panel B). These data suggest that the perturbation of gut microbiota caused by vancomycin affects levels of IFN-gamma-producing CD8+ and CD4+ T-cells. Cohousing with mice that did not receive antibiotic treatment probably induced a bacterial perturbation that increased oncolytic virotherapy efficacy.

A

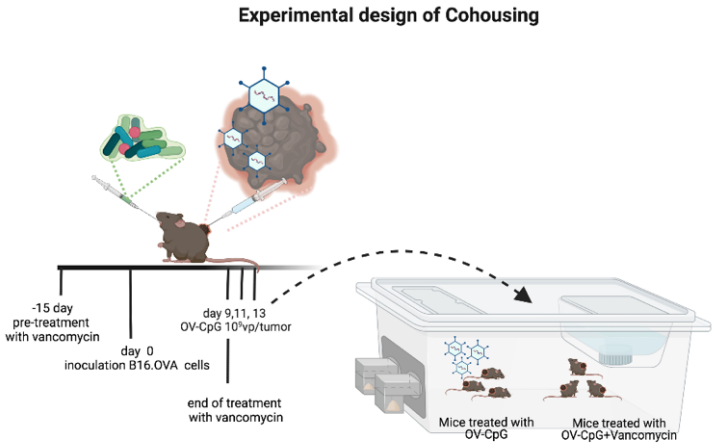
Experimental design of Cohousing
-15 day
pre-treatment
with vancomycin
day 0
inoculation B16.OVA cells
day 9,11, 13
OV-CpG 10^6vp/tumor
end of treatment
with vancomycin
Mice treated with
OV-CpG
Mice treated with
OV-CpG+Vancomycin

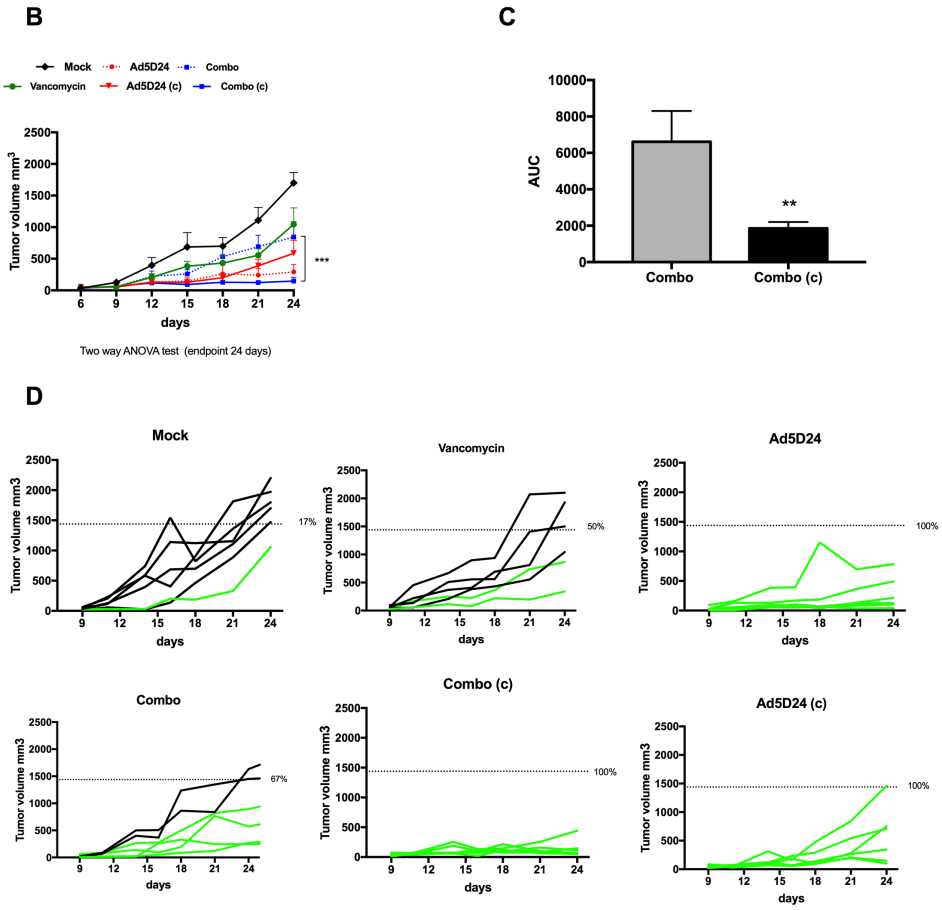
B
Mock
Ad5D24
Combo
Vancomycin
Ad5D24 (c)
Combo (c)
Tumor volume mm3
days
***
Two way ANOVA test (endpoint 24 days)
C
AUC
**
Combo
Combo (c)
D
Mock
Vancomycin
Ad5D24
Combo
Combo (c)
Ad5D24 (c)
17%
50%
100%
67%
100%
100%

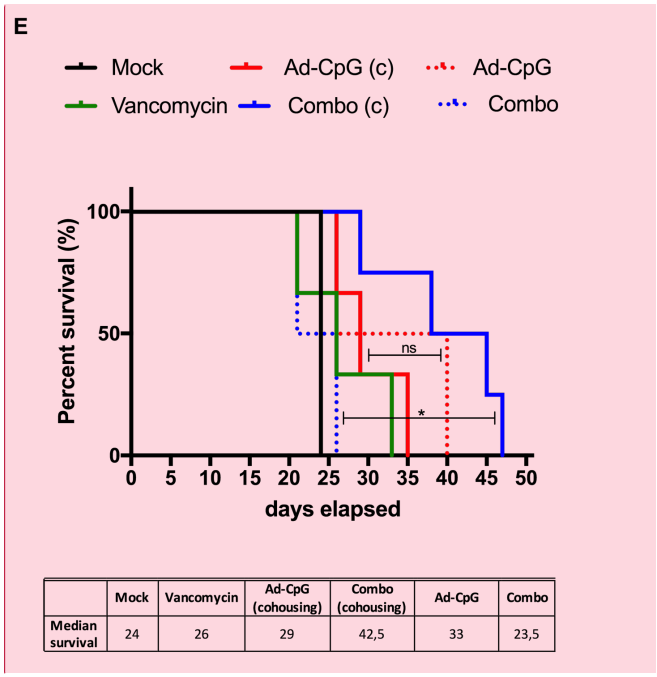

	Mock	Vancomycin	Ad-CpG (cohousing)	Combo (cohousing)	Ad-CpG	Combo
Median survival	24	26	29	42,5	33	23,5

Commentato [LT4]: Correction 6

Figure 9. Differences in melanoma outgrowth of mice treated with oncolytic vaccine and vancomycin and of Ad-CpG-treated group are eliminated when mice are cohoused. A) Experimental design of cohousing: antibiotic vancomycin was administered by oral gavage every two days, 15 days before tumor implantation. At day 0, $3x10^5$ B16.OVA cells were injected in the flank of female C57BL/6J mice (n=6 per group). Ad-CpG was administered intratumorally on days 9, 11 and 13. After the third injection of virus, we cohoused the group treated with combined regiment, Ad-CpG + vancomycin with Ad-CpG-treated control group. The groups involved in the cohousing were indicated with (c) **B)** tumor-bearing mice (n=5 per group) were treated with saline solution (Mock), 100 µl of vancomycin (10mg/ml), $1x10^9$ vp/tumor of Ad-CpG and with a combination of Ad-CpG + vancomycin. Tumor size was measured at each time point for each mice; results are graphed as mean for each treatment groups ± SEM; statistical difference has been determined with 2way ANOVA (*p < 0.05, **p < 0.005). **C)** The area under the curves relative to the tumor growth of mice was calculated and plotted as the mean ± SEM **D)** The single tumor growth curves for each

tumor treated in every mouse and one graph for each group are reported (n=6 animals per group). Responders are defined in percentage (displayed next to each graph) as mice that show an absolute volume lower than 1438,631mm^3. The tumors responder are represented by green curves and tumors non-responder are represented by black curves. **E)** Survival curve relative to the experiment in panel B. The median survival of each group is reported in the table below the graph. The log rank Mantel-Cox analysis was used to calculate the p value (p value =0,0276) of the survival curves.

Commentato [LT5]: Correction 3

Commentato [LT6]: Correction 6

A

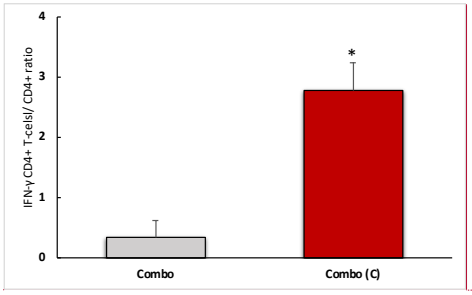

Commentato [LT7]: Correction 7

B

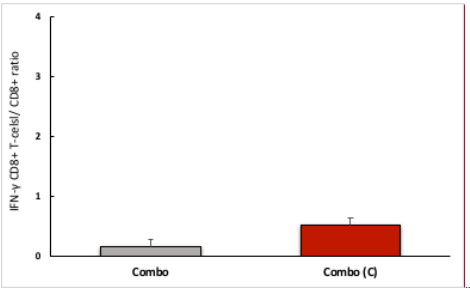

Commentato [LT8]: Correction 7

Figure 10. Treatment with vancomycin affects levels of IFN-gamma-producing CD8+ and CD4+ T-cells. A) Flow cytometry analysis of IFN-gamma CD4+/CD4+ T-cells ratio**. B**) Flow cytometry analysis of IFN-gamma CD8+/CD8+ T-cells ratio. The statistical significance was examined by the Student's t-test and the asterisks indicate statistical significance (***p<0.001; **p<0.01; *p<0.05) compared to control group, treated with combined regimen (Combo) and kept isolated. The vertical lines indicate the standard deviation (SD).Both groups analyzed received combined regimen and were kept respectively isolated (Combo) and cohoused (Combo C).

4.3 Bifidobacterium spp. exert improves oncolytic adenovirus efficacy by reducing tumor-infiltrating T-reg lymphocytes.

Recently, investigators have linked abundance of specific bacteria to immunotherapy success and in fact several clinical studies are currently investigating the therapeutic potential of gut microbiota manipulation in cancer patients through the supplementation of probiotics, along with their anticancer regimen. Commensal bacteria, such as *Bifidobacterium*, have been shown to modulate dendritic cells (DCs) function resulting in enhanced antitumor T-cell activity. Considering that our viral agent Ad-CpG elicits a strong T CD8 mediated immune response in our melanoma cell line, we choose *Bifidobacterium spp*. a probiotic, in order to evaluate the possible synergistic antitumor activity . We then decided to inoculate syngeneic B16-OVA melanoma cells in female C57BL/6J and treat them with Ad-CpG alone or in combination with a *Bifidobacterium* cocktail (Bifidus), as explained in the material and methods section. We observed an increased response to the oncolytic adenoviral therapy in mice that received also Bifidus treatment (Figure 11, panel A) compared to groups treated with Ad-CpG alone and saline. We observed a significantly slower growth kinetics, as represented by the AUC analysis, in mice treated with the combination therapy (Ad-CpG + Bifidus) compared to those treated with Ad-CpG alone (Figure 11, panel B). Interestingly, oral administration of Bifidus by itself resulted in a slightly slower tumor progression compare to mock-treated mice; a different growing trend can be appreciated considering the tumor growth curves for single mouse treated (40% responders, Figure 11, panel C). These surprising results confirmed that Bifidus affects the tumor progression also because of its immuno-stimulatory power and seems to have a synergistic action with oncolytic adenovirus Ad-CpG. Considering the potent immunogenicity of Ad-CpG and the limitation of human serotype 5-based oncolytic adenoviruses that do not induce significant oncolytic effects in murine cells due to species-specific incompatibility, the observed effect most probably relies on the activation of the immune system. We think that this effect resulted also by a positive perturbation of microbiome caused by Bifidus as opposed to that caused by antibiotic vancomycin. We then analyzed lymphocytes in spleens and tumors collected from all groups. We observed a consistent percentage of CD8+ T-cells in spleens from mice treated with Ad-CpG and with the combination therapy (Figure 12, panel A). No differences were appreciated for CD4+ T-

cells between different treatments; however, a reduced percentage of T-reg lymphocytes was observed in the spleen and in tumor samples of mice treated with the combination therapy (Figure 12, panel B and C, respectively). This reduction is even more significant in mice that received only Bifidus supplementation. These data suggest that Bifidus, alters the composition of the gut microbiota and is able to alter T-reg-lymphocytes subset intratumoral infiltration.

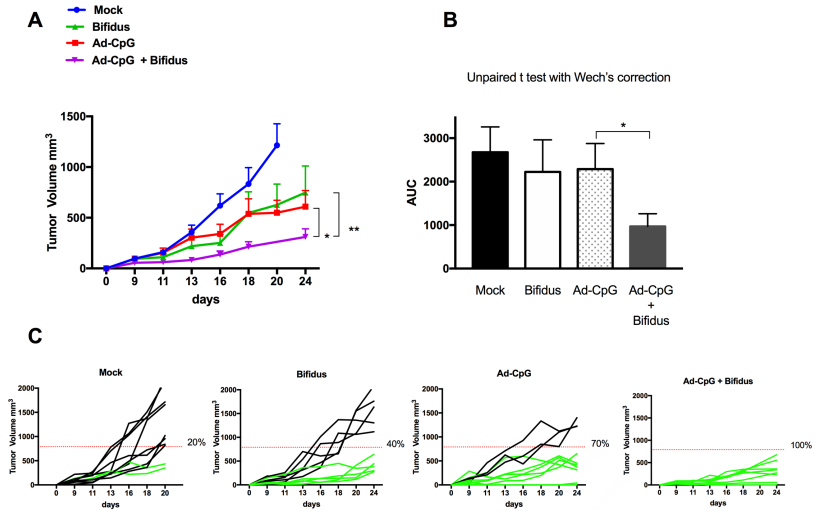

Figure 11. Co-administration of the oncolytic virus and Bifidobacterium spp. reduces the melanoma growth in a syngeneic C57BL/6J mouse model. 3x10^5 B16.OVA cells were injected in both flanks of female C57BL/6 mice (n=5 per group) and both tumors were treated simultaneously, in order to monitor their local tumor growth. Ad-CpG was administered intratumorally on days 9, 11 and 13; Bifidobacterium spp.cocktail (Bifidus) was added to the drinking water 10 days before the cancer cell inoculation and at day 9, 11, 13, 15, 17 and 19. **A)** tumor-bearing mice (n=5 per group) were treated with saline solution (mock), 10^9 CFU/ml of Bifidobacterium spp.cocktail (Bifidus), 1x10^9 vp/tumor of Ad-CpG and with a combination of the two monotherapies (Ad-CpG + Bifidus). Tumor size, of both tumor burdens, was measured at each time point for each mice; results are

Commentato [LT9]: Correction 2

Commentato [LT10]: Correction 8

graphed as mean for each treatment groups ±SEM ; statistical difference has been determined with 2way ANOVA (*p < 0.05, **p < 0.005). **B)** The area under the curves relative to the tumor growth of mice treated was calculated and plotted as the mean ± SEM. **C)** The single tumor growth curves for each tumor treated in every mouse and one graph for each group are reported (n = 10 animals per group). Responders are defined in percentage (displayed next to each graph) as mice that show an absolute volume lower than 790,74 mm^3. The tumors responder are represented by green curves and tumors non-responder are represented by black curves.

Commentato [LT11]: Correction 3

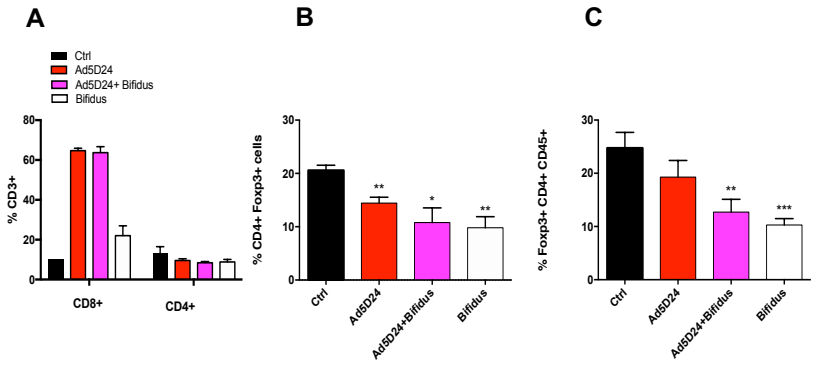

Figure 12. Tumor treated with oncolytic virus and Bifidobacterium spp. showed a less activity of CD4⁺ regulatory T-cells. A) Expression of the markers CD8+ and CD4+ on the surface of CD3+ T-lymphocytes isolated from spleen of mice treated. **B)** Expression of the marker Foxp3+ on the surface of CD4+ CD3+ T-lymphocytes isolated from spleen **C)** Expression of the marker Foxp3+ on the surface of CD4+ CD45+ T-lymphocytes isolated from tumor. Statistically significant differences were determined with Student's t-test; *p<0.05, **p<0.005, ***p< 0.001

Gating strategy

Commentato [LT12]: Correction 9

Viable lymphocytes (LYM)

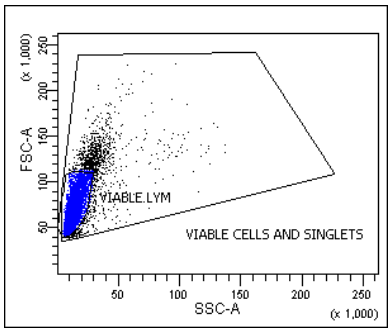

CD3+ T LYM

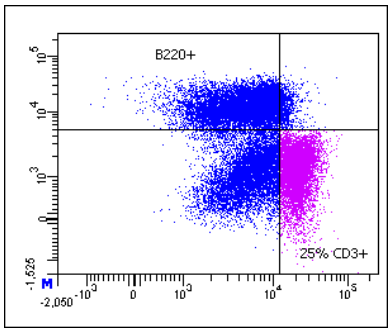

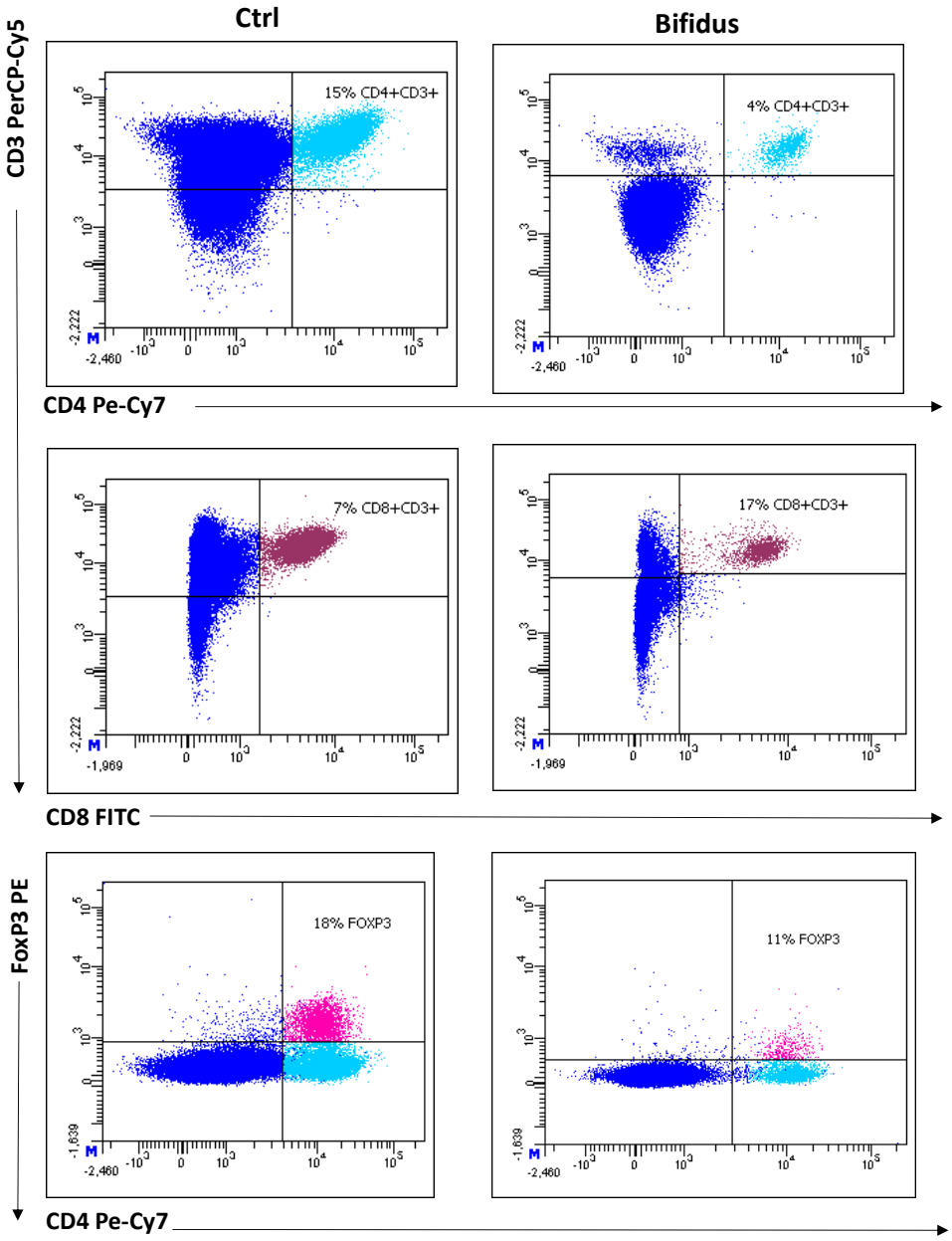
Ctrl
Bifidus
CD3 PerCP-Cy5
15% CD4+CD3+
4% CD4+CD3+
CD4 Pe-Cy7
7% CD8+CD3+
17% CD8+CD3+
CD8 FITC
FoxP3 PE
18% FOXP3
11% FOXP3
CD4 Pe-Cy7

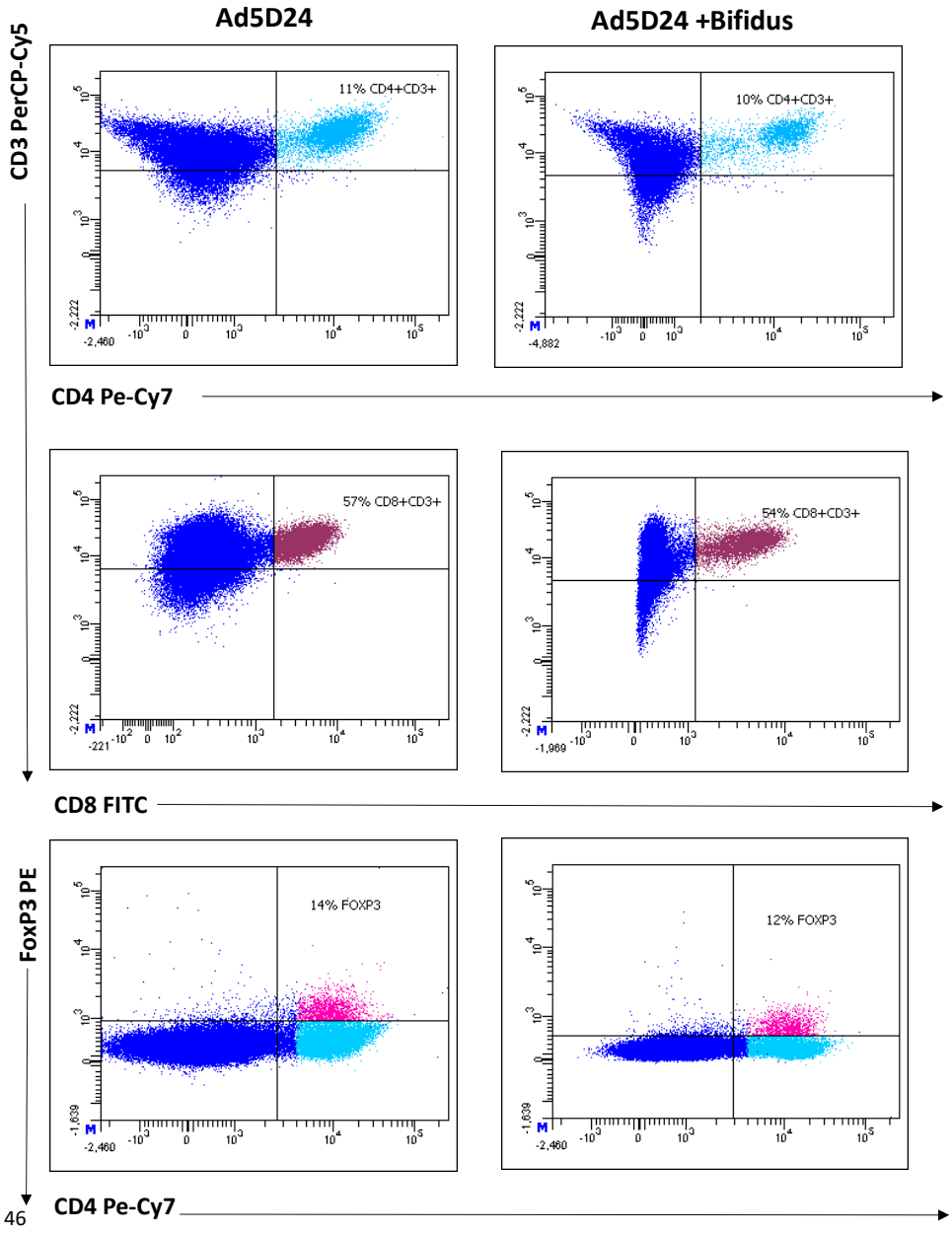
Ad5D24
Ad5D24 +Bifidus
CD3 PerCP-Cy5
11% CD4+CD3+
10% CD4+CD3+
CD4 Pe-Cy7
57% CD8+CD3+
54% CD8+CD3+
CD8 FITC
FoxP3 PE
14% FOXP3
12% FOXP3
CD4 Pe-Cy7

Figure 13. Flow cytometry representative plots of analysis of Foxp3+ CD4+ CD3 lymphocytes. The panel below represents the quadrant gating strategy that has been used for all spleen samples collected. The lymphocytes gate (blue color population indicated as LYM, left panel) was obtained using physical parameters such as (Side scatter) SSC-A and (Forward scatter) FSC-A and then T lymphocytes were gated on CD3+ cells. right panel). B220 was used to select B lymphocytes on lymphocytes. For each treatment, we report the flow cytometry representative plots of CD8+CD3+, CD4+CD3+ and Foxp3+ CD4+ CD3+ T lymphocytes.

4 4 .Pre-immunized splenocytes with oncolytic vaccine and bifidobacterium reduced melanoma cells survival in vitro

In order to evaluate the presence of an immunological memory against the tumor, we collected spleen samples from each group and performed a co-culture assay with B16-OVA cells and pre-immunized murine lymphocytes to assess their ability to induce cancer cell death. This experiment is a preliminary assessment of the anti-tumor effect of lymphocytes from mice treated with Ad-CpG, Bifidus and their combination on cancer cells. Viability of B16-OVA treated with splenocytes derived from mice treated with the combination therapy was significantly lower (56.92% of untreated cells) compared to cells co-cultured with splenocytes obtained from mice that received the other treatments (Figure 14, panel A). Cytotoxic effect was determined by Lactate dehydrogenase (LDH) release in the medium and also revealed an increased cell death in cells co-cultured with splenocytes derived from combination therapy-treated mice (Figure14, panel B).Despite these preliminary results, we can't exclude the possibility that the level of activation of splenocytes collected from Ad-CpG and Bifidobacterium-treated mice could be due to non-specific killing mechanism by T cells activated, by the combined regimen. In conclusion, the increased cell death observed in co-culture assay (Figure 14, panel A), is not sufficient to assert that the combined regimen is so immunogenic as much as to elicit a specific activation of T cells, that in turn destroy cancer cells.

Commentato [LT13]: Correction 10

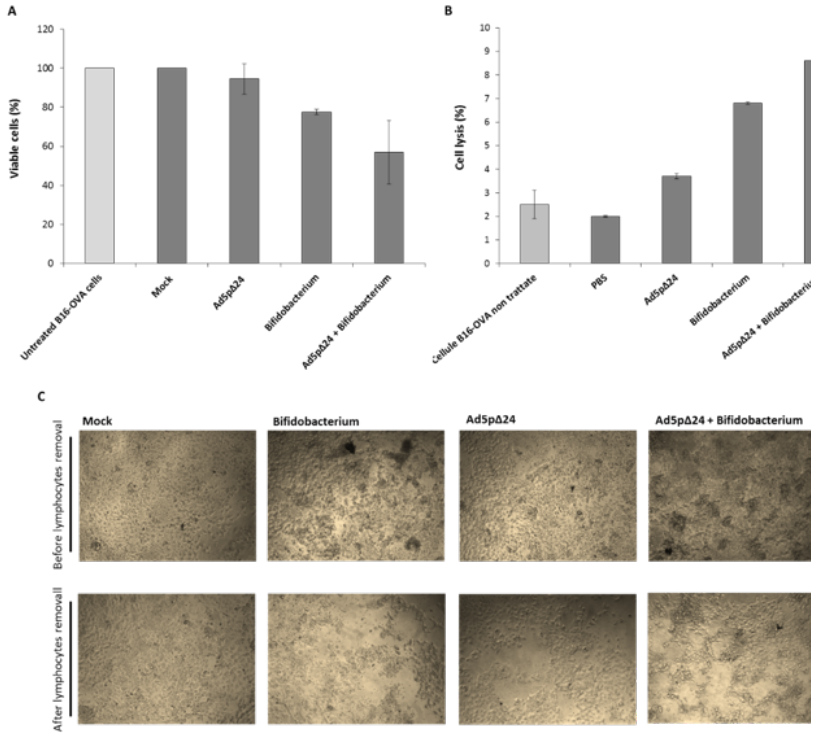

Figure 14. Pre-immunized splenocytes with Ad-CpG and Bifidobacterium activated against melanoma cells. B16-OVA cells were incubated with or without murine lymphocytes isolated from spleens of mice, previously treated with PBS, oncolytic Ad-CpG, Bifidobacterium or combination of virus and Bifidobacterium for 48 hours. **A)** Cell viability is reported as percentage of viable cells compared to untreated B16-OVA tumor cells (gray bar) **B)** tumor cells lysis was determined by measurement of LDH release in culture medium. Levels of LDH released by cancer cells are expressed as a percentage, compared to untreated cells. **C)** Representative images of B16-OVA cells untreated or treated as indicated were acquired after splenocyte removal. The experiments were performed in triplicate and statistical significance was examined by the Student's t-test. The asterisks indicate statistical significance (***p<0.001; **p<0.01; *p<0.05) compared to untreated cells. The vertical lines indicate the standard deviation (SD).

4.5 Treatments with Ad-CpG alone and in combination with Bifidus cause perturbations of mice fecal microbiome.

In order to better characterize the effect of oncolytic adenovirus Ad-CpG alone and in combination with Bifidus, we decided to investigate the fecal microbiome profiles of mice treated. The animals involved in this bacterial analysis were the same used in the experiment previously showed (paragraph 4.1, Figure 11). We monitored fecal bacterial content over time in treated mice with 16S ribosomal RNAs (rRNAs) analysis using Next generation sequencing (NGS). The stool samples collection occurred in specific timepoints:
Day-10: starting pretreatment with Bifidus
Day 0: cancer cell inoculation
Day18: five days after the last injection of adenovirus
Day 20: endpoint of mock group

Ninety-three fecal samples were collected and processed for microbiome evaluation. All samples were processed as described under methods and sequenced in one NGS run. In order to deeply investigate a possible link between the gut microbiome composition and the different therapeutic regimen, we sought possible differences between the microbial profiles of groups. According to the Kruskal-Wallis test among the four time points for each treatment, distinct phyla were identified such as Verrucomicrobia, Tenericutes, Proteobacteria, Fusobacteria, Firmicutes, Deferribacteres, Cyanobacteria, Bacteroidetes and Actinobacteria (Figure 15). In the group untreated (Mock), Tenericutes and Actinobacteria were the phyla significantly different between the four time points and in Bifidus-treated group were Proteobacteria and Actinobacteria. On the contrary, in the group treated with Ad-CpG Firmicutes and Actinobacteria were significantly different between the four time points and in the group treated with Ad-CpG + BIF as additional phyla Deferribacteres Tenericutes and Cyanobacteria were identified (Figure 15). Interestingly, the microbial profile of both groups (Ad-CpG and Ad-CpG + BIF), treated with Ad-CpG was mainly characterized by Firmicutes; considering the timepoint Day 18, the relative abundance of Firmicutes phylum was about 63% (Figure 15).
By Dunn's test, a post hoc non parametric test applied to the Kruskal-Wallis significant amplicon sequence variants (ASVs), we performed multiple pairwise tests in order to

identify, between which time pairs the phyla differentially abundant were significant. As reported in the Table 1, Tenericutes and Actinobacteria phyla resulted significantly abundance between the earlier (Day -10) and later (Day 18 and Day 20) timepoints suggesting that their relative abundance was independent of tumor growth both in mock and Bifidus-treated group. In both groups treated with Ad-CpG, the abundance of Actinobacteria was significant between Day -10 to Day 18, indicating that the pretreatment with Bifidus did not affect its richness. In Ad-CpG treated group, Firmicutes phylum was significantly abundance between the Day 0 and Day 18, when differences between tumor grow curves were well appreciated, as shown in Figure 11, panel A. Similar result was confirmed in Ad-CpG + BIF -treated group, in which the relative abundance of Firmicutes was significant also between Day -10 and the endpoint (Day 20) (Table 1).These data confirmed that melanoma-bearing mice treated with Ad-CpG were characterized by an enrichment of Firmicutes in their fecal microbiota. The relative abundance of differentially abundant genera ($p<0.05$) for each study group, according to the Kruskal-Wallis test among the four time points, was reported in Table 2.

In fecal bacterial content of mice treated with Ad-CpG, the genera identified and belonging to *Firmicutes* phylum, were *Faecalibaculum*, *Lachnospiraceae_NK4A136*, *Lachnospiraceae_UCG-001*, *Roseburia*, *Ruminiclostridium* and *Ruminiclostridium_9*. In addition to these genera, *Turicibacter*, *Oscillibacter* and *Lachnoclostridium* were identified in the group treated with Ad-CpG + BIF. *Bifidobacterium*, belonging to Actinobacteria phylum, was identified in all groups, but with a relative abundance of about 10% in the group treated with Bifidus, compared to relative abundance of 4,9% observed in the group treated with Ad-CpG + BIF (Table 2).

At genus level, we have identified a specific fecal microbiota profile in both groups treated with Ad-CpG. Specifically, *Faecalibaculum*, *Lachnospiraceae_NK4A136* and *Bifidobacterium* genera showed a relative abundance greater than 2% in fecal bacterial composition of groups treated with oncolytic adenovirus Ad-CpG (Figure 16).

A specific strain of *Faecalibaculum* (*Faecalibaculum rodentium*) was identified as anti-tumorigenic bacterial strains with strong diagnostic, therapeutic and translational potential. *Faecalibaculum rodentium* was able to inhibit cancer cell growth in a spontaneous mouse model of colon cancer, producing the SCFA butyrate that contributed to control protein acetylation and tumor cell proliferation in mouse and human settings (105). Interesting findings demonstrated Lachnospiraceae *NK4A136* group had the potential to be a probiotic, in fact the diminished amount of probiotic *Lachnospiraceae*

NK4A136 group in high fat diet (HFD)-fed mice was restored to the level comparable to those in controls after the dietary shift to a balanced one (106). Finally, an unexpected role for commensal *Bifidobacterium* in enhancing antitumor immunity in vivo, was demonstrated by Sivan et al (89). Bifidobacterium-derived signals modulate the activation of DCs which in turn supports improved effector function of tumor-specific CD8+ T cells. Acting as an adjuvant, *Bifidobacterium* probiotic is an optimum candidate to combine with immunotherapeutic strategies. These data support the hypothesis that treatment of tumors with Ad-CpG, significantly affects fecal microbiota composition in preclinical model of melanoma.

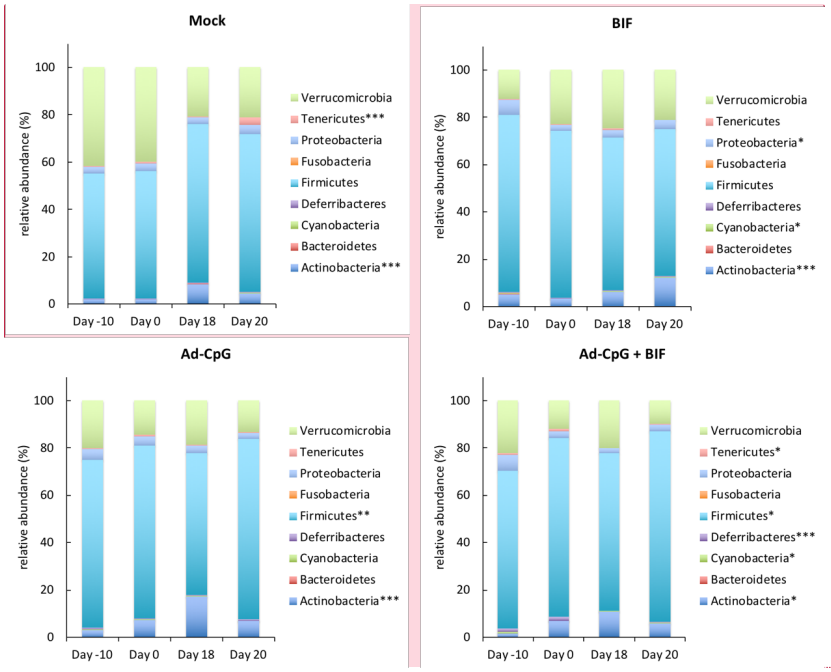

Figure 15. Treatment of tumor with oncolytic adenovirus Ad-CpG is characterized by an increase of Firmicutes phylum in the murine fecal microbiome. The barplots show Kruskal Wallis test results on amplicon sequence variants (ASVs) grouped in phyla for each study group (Mock, BIF, Ad-CpG and Ad-CpG + BIF), over the time points (Day-10, Day 0, Day 18 and Day 20). Each column in the plot represents a time point and each color in the column represents the percentage of relative abundance. The phyla significantly (***p<0.001; **p<0.01; *p<0.05) different between the four time points and for each treatment, were shown in each panel alongside each barplot graph.

Commentato [LT14]: Correction 12 and 13

Treatment	Phylum	Comparison Timepoints (Days)	Z	p-value unadjusted	p-value adjusted
Mock	Tenericutes	-10 to 20	-3,527848	0,00041895	0,00251371
		0 to 20	-2,244994	0,02476849	0,04953698
	Actinobacteria	-10 to 18	-3,3140394	0,00091959	0,00275876
		0 to 18	-3,3674917	0,00075855	0,00455132
BIF	Actinobacteria	0 to 20	-3,3140394	0,00091959	0,00551751
	Proteobacteria	-10 to 0	2,7260647	0,00640944	0,03845666
		-10 to 18	2,5657079	0,01029655	0,03088965
	Cyanobacteria	-10 to 0	2,3518989	0,01867785	0,05603355
Ad-CpG	Actinobacteria	-10 to 18	-3,3674916	0,00075855	0,00455132
	Firmicutes	0 to 18	2,6191602	0,00881466	0,02644396
		18 to 20	-3,1002304	0,0019337	0,01160221
Ad-CpG + BIF	Actinobacteria	-10 to 18	2,8864214	0,0038965	0,023379
	Firmicutes	-10 to 20	-2,4053512	0,01615693	0,04847079

Ad-CpG + BIF	**Deferribacteres**	-10 to 18	2,93987366	0,00328346	0,01970077
		0 to 18	2,88642141	0,0038965	0,0116895
	Cyanobacteria	-10 to 0	2,7805624	0,00542648	0,03255889
		-10 to 18	2,4597283	0,01390422	0,04171267
	Tenericutes	-10 to 18	2,4053512	0,01615693	0,04847079
		0 to 18	2,6726124	0,00752632	0,04515789

Table 1. Results of Dunn's test, applied to the Kruskal-Wallis significant amplicon sequence variants (ASVs); the phyla shown in the table for each treatment, were obtained from significant comparisons between time pairs, according to the Benjamini and Hochberg's false discovery rate (FDR) correction (BH) adjusted p-value < 0.05.

Commentato [LT15]: Correction 15

Treatment	Genera	Timepoints (Days)			
		Relative abundance (%)			
Mock	Anaeroplasma	Day -10 0,009	Day 0 0,444	Day 18 0,331	Day 20 3,010
	Bifidobacterium	1,054	1,260	7,375	3,887
	Faecalibaculum	6,575	11,116	27,624	11,158
	Desulfovibrio	1,699	1,314	0,332	0,526
BIF	Coriobacteriaceae_UCG-002	0,161	0,211	0,376	1,791
	Bifidobacterium	4,574	2,382	5,598	10,029
	Parasutterella	2,882	0,237	1,104	2,154
	Desulfovibrio	1,289	1,931	0,522	0,641
Ad-CpG	Bifidobacterium	2,367	6,199	15,505	5,878
	Faecalibaculum	10,879	13,718	27,271	22,395

Ad-CpG	**Lachnospiraceae_NK4A136**	16,073	12,494	6,562	19,086
	Lachnospiraceae_UCG-001	0,403	0,717	0,303	1,450
	Lactobacillus	14,456	19,185	11,309	4,201
	Roseburia	1,590	1,111	0,441	1,782
	Ruminiclostridium	0,876	0,759	0,346	1,336
	Ruminiclostridium_9	1,510	1,093	0,578	1,669
Ad-CpG + BIF	**Bifidobacterium**	1,260	5,648	9,156	4,925
	Faecalibaculum	4,001	22,111	34,477	11,502
	Lachnospiraceae_NK4A136	18,355	17,796	4,903	21,342
	Lachnospiraceae_UCG-001	3,359	1,296	0,740	0,769
	Roseburia	0,697	1,272	0,340	2,205
	Ruminiclostridium	1,331	0,991	0,310	1,787
	Ruminiclostridium_9	1,413	1,387	0,457	1,232

Ad-CpG + BIF	**Lachnoclostridium**	0,648	0,814	0,315	1,261
	Mucispirillum	1,441	1,699	0,077	0,493
	Oscillibacter	0,873	0,822	0,235	1,426
	Anaeroplasma	0,769	1,143	0,102	0,333
	Turicibacter	5,342	1,036	2,576	3,516

Table 2. The table shows the relative abundances of differentially abundant genera ($p<0.05$) for each study group (Mock, BIF, Ad-CpG and Ad-CpG + BIF), according to the Kruskal-Wallis test among the four time points (Day-10, Day 0, Day 18 and Day 20).

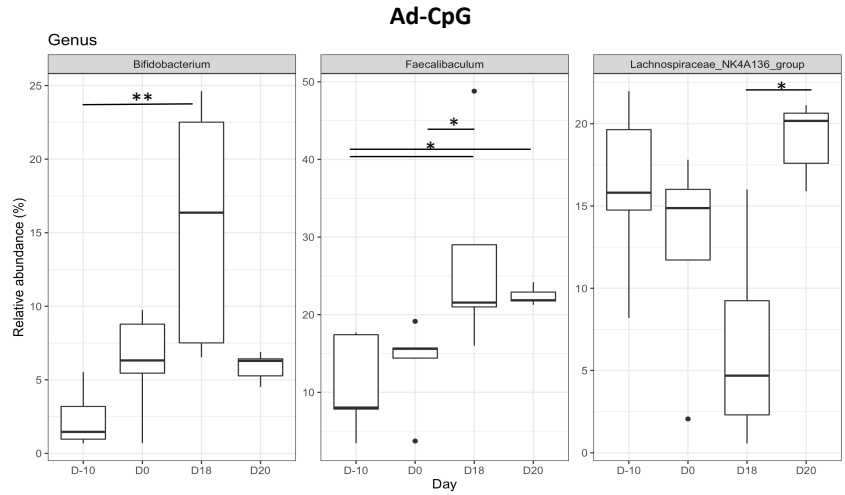
Ad-CpG
Genus
Bifidobacterium
Faecalibaculum
Lachnospiraceae_NK4A136_group
Relative abundance (%)
D-10
D0
D18
D20
Day

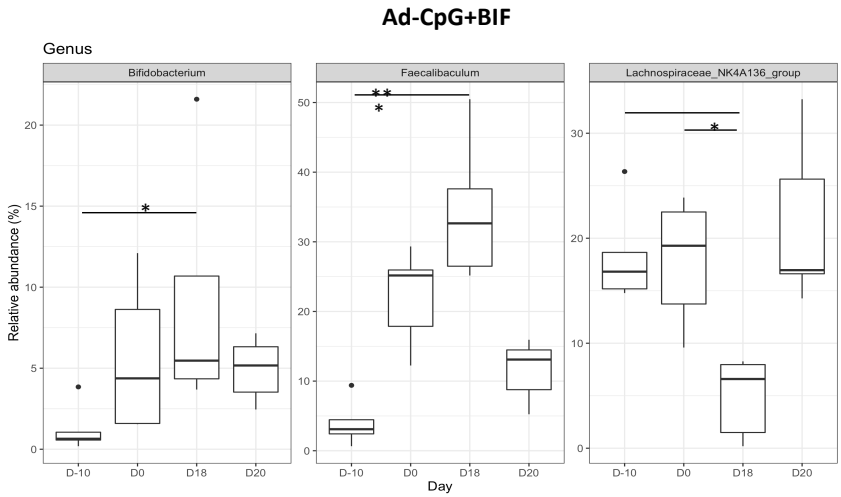
Ad-CpG+BIF
Genus
Bifidobacterium
Faecalibaculum
Lachnospiraceae_NK4A136_group
Relative abundance (%)
D-10
D0
D18
D20
Day

Figure 16. Treatment of tumor with oncolytic adenovirus Ad-CpG is characterized by a specific fecal composition at genus level. The three genera with a relative abundance > 2% shown in the box plots were in common between Ad-CpG and Ad-CpG + BIF groups .Middle line in boxes represents the median; lower box bounds the first quartile; upper box bounds the 3rd quartile. Whiskers represent the 95% confidence interval of the mean. The significance of distribution differences has been calculated applying the Kruskal-Wallis test, Dunn's post-hoc test and Benjamini-Hochberg p-value adjustment (* $p < 0.05$; ** $p < 0.01$; *** $p < 0.005$).

Discussion

Currently, therapies targeting immune checkpoint such as programmed cell death protein 1/programmed cell death ligand 1 (PD-1 /PD-L1) or cytotoxic T-lymphocyte antigen-4 (CTLA-4) are the focus of cancer immunotherapy and are widely applied in clinical treatments of various tumors. Owing to relatively low overall response rate, to date its efficacy has not been consistent probably because of a number of environmental and genetic factors influencing the outcome. Without doubt gut microbiome is an emerging element responsible of this inhomogeneous response, because of its great impact on the tumor response to ICIs therapy (79,89,94-95). So, given the great scientific interest common shared by many researchers in learning in depth the link between microbiome and outcome variability to ICIs therapy, we focused our study in a contest never investigated: the possible relation between gut microbiome and viro-immunotherapy efficacy. Considering OVs therapy as a possible complement to increase success of ICIs immunotherapy, we hypothesized that intestinal microbiota could influence OVs therapy efficacy.

To answer our question, we used an oncolytic adenovirus enriched with 18 CpG island (Ad-CpG, 97) (Figure 4) able to overstimulate TLR9 and triggers a more robust immune response. This vector has been successfully evaluated previously, using a syngeneic melanoma model based on the inoculation of B16-OVA cells in C57BL/6J mice (25); this melanoma responds to ICIs therapy and is sensitive to microbiota perturbation (5,11) and in addition the tumor model allows an accurate assessment of tumor specific T-cell responses because of the presence of an intact immune system.

In order to evaluate whether gut microbiota could affect the antitumoral activity of the Ad-CpG, we reset the gut bacterial content, pre-treating mice with the antibiotic vancomycin which mostly eliminates gram-positive bacteria, had been previously effectively used for the same purpose (79). We found that pre-treatment with vancomycin reduced the efficacy of treatment with Ad-CpG: these mice had a faster tumor progression compared to mice treated only with Ad-CpG. We confirmed that antibiotic-mediated effects during cancer treatments are context dependent (69) and can be either beneficial (79) or harmful, as in our experiments.

The negative impact of vancomycin on antitumoral activity of Ad-CpG was confirmed by a reduced count of IFN-gamma+ CD8+ TILs in pretreated mice compared to the control group (Figure 7, panels A- B). We concluded that antibiotic-associated dysbiosis altered the

immunomodulatory function of the intestine and reduced efficacy of antitumoral immune responses elicited by OVs, as observed for tumors in antibiotic-treated mice did not respond to CTLA blockade (79). In order to further support this hypothesis, we cohoused a group of mice pretreated with vancomycin and then treated with Ad-CpG (combined regimen) with a group of mice that received only the oncolytic adenovirus Ad-CpG, as indicated in the experimental design (Figure 9, panel A). Because of mice coprophagy and grooming behavior, cohousing has been identified as simplest method to transfer the microbiota between mice (107). As expected, cohousing significantly reduced differences in tumor growth between mice treated with the combined regimen compared to mice treated with Ad-CpG alone, indicating that a positive perturbation and possibly a restoration of gut microbiota occurred (Figure 9, panel B); in fact the percentage of tumors that completely respond to Ad-CpG therapy, even if was pre-treated with vancomycin was about of 100% compared to group treated with same combined regimen and kept isolated (percentage of responder about of 67%) (Figure 9, panel D).

Additionally, mice pretreated with vancomycin and Ad-CpG and successfully cohoused with mice that did not receive the antibiotic had an increased overall survival (median survival 40 days) compared to mice treated with the same regimen and kept isolated (median survival 25 days) (Figure 9, panel E). We believe that the statement of vancomycin-induced dysbiosis at intestinal level likely induced an expansion of some bacteria poorly immunogenic that negatively affect the adjuvant activity of Ad-CpG, reducing its antitumoral efficacy as shown by different levels of IFN-gamma-producing CD8+ and CD4+ T-cells between groups (Figure 10, panels A-B). However, we used an Ad-CpG for this study, therefore this effect needs to be evaluated in OVs different type of OVs.

Recent studies have shown that stimulatory interactions between microbiota and host immune system may be due to *Bifidobacterium*, as positive regulator of antitumoral immunity in vivo causing an induction of pro-inflammatory signals in innate immune cells (89). We therefore decided to evaluate the possible immunomodulatory activity of *Bifidobacterium* probiotic (Bifidus) combined with Ad-CpG therapy in our melanoma mouse model. *Bifidobacterium* was chosen as agent for microbiota modulation because of its capability to enhance-protective immunity against tumors, in combination with anti-PD-L1 therapy (89). Furthermore *Bifidobacterium* along with *Akkermansia muciniphila*, *Ruminococcus* and *Eubacterium* were found to positively correlate with ICI response, and in fact they constitute a real favorable intestinal microbiota (69,95). Our data strongly indicate that Bifidus treatment increases the response to Ad-CpG compared to mice

Commentato [LT16]: Correction 16

treated with Ad-CpG alone and PBS, confirming its potential immunomodulatory activity. (Figure 11, panel A). Furthermore, we observed a reduced percentage of T-reg lymphocytes in spleen and tumor samples from mice treated with Bifidus and Ad-CpG, confirming that Bifidus exerts an immunomodulatory activity (89) and possibly affect the tumor-induced immunosuppression (Figure 12, panels A-C). A preliminary assessment of levels of activation against melanoma cells of combined regimen pre-immunized splenocytes, suggested the presence of T cell-mediated killing and an immunological memory. This effect could not be directly connected to the presence of Ad-CpG combined with Biifdus supplementation (Figure 14).

Commentato [LT17]: Correction 10

On the basis of our results, we observed that Ad-CpG efficacy is affected by vancomycin-induced perturbations in the gut microbiome. In other words, the level of antitumoral immune response elicited by Ad-CpG, worsen in vancomycin recipient-mice, as shown by a decrease of tumor-infiltrating IFNγ+ CD8+T-cell.

As previously shown, antibiotic-mediated gut microbiota alteration reduces some beneficial bacteria taxa altering intestinal anti-Inflammatory and immunomodulatory properties (69,79). These bacterial communities contribute to a healthy host-microorganism balance useful to optimally perform metabolic and immune functions and reduce disease development. The phylogenetic make-up of the bacterial communities in both human and mouse seem to be similar at phylum level, where the two main bacterial phyla of the murine intestinal tract are the Bacteroidetes and the Firmicutes (108), the most predominant phyla in a human healthy gut (109). For this reason, we compared fecal microbiome of mice treated with combined regimen (Ad-CpG+Bifidus) to mice that received a single treatment and a mock group, by DNA sequencing of the 16S rRNA gene in bacteria. Ad-CpG and combined regimen-recipient mice showed a predominance of the Firmicutes phylum in their fecal bacterial content (Figure 15). In Ad-CpG treated group, Firmicutes phylum was significantly abundance between the cancer cell inoculation (Day 0) and Day 18; similarly in Ad-CpG+BIF -treated group, the relative abundance of Firmicutes was significant between the starting pretreatment with Bifidus (Day-10) until the endpoint (Day 20) (Table 1).These data confirmed that melanoma-bearing mice treated with Ad-CpG were characterized by an enrichment of Firmicutes in their fecal microbiota.

These groups showed respectively seven and nine genera belonging to Firmicutes phylum as reported in the Table 2.

Faecalibaculum, *Lachnospiraceae_NK4A136* and *Bifidobacterium* genera, that showed a relative abundance greater than 2% in groups treated with Ad-CpG , represent a specific fecal bacterial composition linked to oncolytic adenoviral therapy (Figure 16). Then we can assert that Ad-CpG treatment, alone and in combination with Bifidus, significantly affects fecal microbiota composition compared to the other groups analyzed.

The gut microbiota perturbation in both groups treated was characterized by an enrichment of the phylum Firmicutes, that creates a favorable and immunologically permissive gut microbiota that contributes to the antitumoral immune responses elicited by Ad-CpG. Therefore, Ad-CpG has the ability to affect the gut microbiota content of mice, promoting a microbial shift versus more beneficial taxa belong to Firmicutes phylum. T-cell activation elicited by the Ad-CpG may be able to mitigate the pro-inflammatory environment caused by the tumor, restoring an eubiosis status in the gut microbiota ecosystem. A similar scenario was observed in groups treated with Ad-CpG and that received supplementation with Bifidus, confirming its potential immunomodulatory activity (89). Considering that OVs therapy is emerging as long-term solution for cancer treatment, the synergistic action of Bifidus could be exploited to design new OVs-based therapy obtaining even more durable benefits.

Our present work has implications in the development of diagnostic and therapeutic strategies that will possibly increase the efficacy of OV-based therapy. Given the present data, it is highly probable that gut microbiome analysis prior to OV-based immunotherapy is going to be a strong predictor of therapeutic efficacy. In addition, combination of probiotic and OVs treatments needs to be thoroughly assessed to further increase efficacy of ICIs immunotherapy. Further studies are necessary to further characterize this phenomenon and identify bacterial species and possible their metabolic products involved in this effect; recent evidence point to a possible mechanism of molecular mimicry (110) or to a possible immunomodulatory effect of bacterial glycan (111) or metabolites, such as butyric acid (112). New mechanistic investigations are focusing on role in modulating and reshaping the host epigenome (113). In particular, this aspect was studied in CRC patients, where gut microbiota represents a proven cause of disease. Several active microbial metabolites have been found to drive carcinogenesis, invasion, and metastasis via modifying the methylation pattern of cancer-related genes along and histone structure in intestinal cells. Some abnormal epigenetic modifications (AKA epimutations) occur in the promoter regions of tumor suppressor genes and proto-oncogenes. These epimutations were reported in CRC and in other malignancies, where many genes such as GATA4,

p16INK4a, MLH1, LKB1, and APC represent common targets (114). Thus, the deep understanding of how epigenetic modifications affected by the gut microbiota take place could offer possible therapeutic targets to prevent and treat CRC (115).

Commentato [LT18]: Correction 19

Conclusions

Although the role of the gut microbiome in modulating immunotherapy efficacy has been widely considered in many types of cancers, its role in the oncolytic immunovirotherapy of solid tumors is never investigated. Evaluating whether gut microbiome could affect the antitumoral activity of oncolytic adenovirus is interesting, because it could provide insights useful to explain the variability in clinical outcomes and then optimize the efficacy of this immunotherapeutic agent. In addition, the eligibility of OV as optimum candidate to combine with ICIs, whose activity is gut microbiome-mediated, increase the utility of this investigation. Therefore, a new scenario along the oncolytic immunotherapy - gut microbiome axis could be identified. Our study is limited to a single OV in a specific syngeneic melanoma model: we therefore understand that these conclusions have not a general value and cannot be applied to other OVs and tumors. Therefore, further studies will be necessary to evaluate the role of intestinal microbiota and its possible perturbations in other tumor models and with additional OVs and, finally, in clinical settings.

References

1. Passarelli A, Mannavola F, Stucci LS, Tucci M, Silvestris F. Immune system and melanoma biology: a balance between immunosurveillance and immune escape. *Oncotarget*. 2017;8(62):106132-106142. Published 2017 Oct 31. doi:10.18632/oncotarget.22190

2. Maio M. Melanoma as a model tumour for immuno-oncology. *Ann Oncol*. 2012;23 Suppl 8:viii10-viii14. doi:10.1093/annonc/mds257

3. Bomar L, Senithilnathan A, Ahn C. Systemic Therapies for Advanced Melanoma. *Dermatol Clin*. 2019;37(4):409-423. doi:10.1016/j.det.2019.05.001

4. Byrne EH, Fisher DE. Immune and molecular correlates in melanoma treated with immune checkpoint blockade. *Cancer*. 2017;123(S11):2143-2153. doi:10.1002/cncr.30444

5. Rastrelli M, Tropea S, Rossi CR, Alaibac M. Melanoma: epidemiology, risk factors, pathogenesis, diagnosis and classification. *In Vivo*. 2014;28(6):1005-1011.

6. Mei XL, Wei FL, Jia LL, Ji YZ. An alternative pathway for cellular protection in BRAF inhibitor resistance in aggressive melanoma type skin cancer. *Chem Biol Interact*. 2020;323:109061. doi:10.1016/j.cbi.2020.109061

7. Reddy BY, Miller DM, Tsao H. Somatic driver mutations in melanoma. *Cancer*. 2017;123(S11):2104-2117. doi:10.1002/cncr.30593

8. Gyorki DE, Callahan M, Wolchok JD, Ariyan CE. The delicate balance of melanoma immunotherapy. *Clin Transl Immunology*. 2013;2(8):e5. Published 2013 Aug 9. doi:10.1038/cti.2013.5

9. Motofei IG. Melanoma and autoimmunity: spontaneous regressions as a possible model for new therapeutic approaches. *Melanoma Res*. 2019;29(3):231-236. doi:10.1097/CMR.0000000000000573

10. M Mittal D, Gubin MM, Schreiber RD, Smyth MJ. New insights into cancer immunoediting and its three component phases--elimination, equilibrium and escape. *Curr Opin Immunol*. 2014;27:16-25. doi:10.1016/j.coi.2014.01.004

11. Mellman I, Coukos G, Dranoff G. Cancer immunotherapy comes of age. *Nature*. 2011;480(7378):480-489. Published 2011 Dec 21. doi:10.1038/nature10673

12. Hui E. Immune checkpoint inhibitors. *J Cell Biol*. 2019;218(3):740-741. doi:10.1083/jcb.201810035

13. Robert C. Is earlier better for melanoma checkpoint blockade?. *Nat Med*. 2018;24(11):1645-1648. doi:10.1038/s41591-018-0250-0

14. Amaria RN, Reddy SM, Tawbi HA, et al. Neoadjuvant immune checkpoint blockade in high-risk resectable melanoma [published correction appears in Nat Med. 2018

Oct 25](published correction appears in Nat Med. 2018 Oct 25;]Nat Med. 2018;24(11):1649-1654. doi:10.1038/s41591-018-0197-1E.

15. Buchbinder EI, Desai A. CTLA-4 and PD-1 Pathways: Similarities, Differences, and Implications of Their Inhibition. *Am J Clin Oncol*. 2016;39(1):98-106. doi:10.1097/COC.0000000000000239

16. Weber J, Mandala M, Del Vecchio M, et al. Adjuvant Nivolumab versus Ipilimumab in Resected Stage III or IV Melanoma. *N Engl J Med*. 2017;377(19):1824-1835. doi:10.1056/NEJMoa1709030

17. Buchbinder EI, Hodi FS. Melanoma in 2015: Immune-checkpoint blockade - durable cancer control. *Nat Rev Clin Oncol*. 2016;13(2):77-78. doi:10.1038/nrclinonc.2015.237

18. Taube JM, Anders RA, Young GD, et al. Colocalization of inflammatory response with B7-h1 expression in human melanocytic lesions supports an adaptive resistance mechanism of immune escape. *Sci Transl Med*. 2012;4(127):127ra37. doi:10.1126/scitranslmed.3003689

19. Topalian SL, Drake CG, Pardoll DM. Immune checkpoint blockade: a common denominator approach to cancer therapy. *Cancer Cell*. 2015;27(4):450-461. doi:10.1016/j.ccell.2015.03.001

20. Iwai Y, Hamanishi J, Chamoto K, Honjo T. Cancer immunotherapies targeting the PD-1 signaling pathway. *J Biomed Sci*. 2017;24(1):26. Published 2017 Apr 4. doi:10.1186/s12929-017-0329-9

21. Robert C, Schachter J, Long GV, et al. Pembrolizumab versus Ipilimumab in Advanced Melanoma. *N Engl J Med*. 2015;372(26):2521-2532. doi:10.1056/NEJMoa1503093

22. Schadendorf D, Hodi FS, Robert C, et al. Pooled Analysis of Long-Term Survival Data From Phase II and Phase III Trials of Ipilimumab in Unresectable or Metastatic Melanoma. *J Clin Oncol*. 2015;33(17):1889-1894. doi:10.1200/JCO.2014.56.2736

23. Feng Y, Roy A, Masson E, Chen TT, Humphrey R, Weber JS. Exposure-response relationships of the efficacy and safety of ipilimumab in patients with advanced melanoma. *Clin Cancer Res*. 2013;19(14):3977-3986. doi:10.1158/1078-0432.CCR-12-3243

24. Bonaventura P, Shekarian T, Alcazer V, et al. Cold Tumors: A Therapeutic Challenge for Immunotherapy. *Front Immunol*. 2019;10:168. Published 2019 Feb 8. doi:10.3389/fimmu.2019.00168

25. Feola S, Capasso C, Fusciello M, et al. Oncolytic vaccines increase the response to PD-L1 blockade in immunogenic and poorly immunogenic tumors. *Oncoimmunology*. 2018;7(8):e1457596. Published 2018 May 7. doi:10.1080/2162402X.2018.1457596

26. Conry RM, Westbrook B, McKee S, Norwood TG. Talimogene laherparepvec: First in class oncolytic virotherapy. *Hum Vaccin Immunother*. 2018;14(4):839-846. doi:10.1080/21645515.2017.1412896

27. Andtbacka RH, Kaufman HL, Collichio F, et al. Talimogene Laherparepvec Improves Durable Response Rate in Patients With Advanced Melanoma. *J Clin Oncol*. 2015;33(25):2780-2788. doi:10.1200/JCO.2014.58.3377

28. Kuryk L, Møller AW, Jaderberg M. Combination of immunogenic oncolytic adenovirus ONCOS-102 with anti-PD-1 pembrolizumab exhibits synergistic antitumor effect in humanized A2058 melanoma huNOG mouse model. *Oncoimmunology*. 2018;8(2):e1532763. Published 2018 Oct 29. doi:10.1080/2162402X.2018.1532763

29. Bradley S, Jakes AD, Harrington K, Pandha H, Melcher A, Errington-Mais F. Applications of coxsackievirus A21 in oncology. *Oncolytic Virother*. 2014;3:47-55. Published 2014 Apr 10. doi:10.2147/OV.S56322

30. Bramante S, Kaufmann JK, Veckman V, et al. Treatment of melanoma with a serotype 5/3 chimeric oncolytic adenovirus coding for GM-CSF: Results in vitro, in rodents and in humans. *Int J Cancer*. 2015;137(7):1775-1783. doi:10.1002/ijc.29536

31. Koski A, Kangasniemi L, Escutenaire S, et al. Treatment of cancer patients with a serotype 5/3 chimeric oncolytic adenovirus expressing GMCSF. *Mol Ther*. 2010;18(10):1874-1884. doi:10.1038/mt.2010.161

32. Cerullo V, Vähä-Koskela M, Hemminki A. Oncolytic adenoviruses: A potent form of tumor immunovirotherapy. *Oncoimmunology*. 2012;1(6):979-981. doi:10.4161/onci.20172

33. Shafren DR, Dorahy DJ, Ingham RA, Burns GF, Barry RD. Coxsackievirus A21 binds to decay-accelerating factor but requires intercellular adhesion molecule 1 for cell entry. *J Virol*. 1997;71(6):4736-4743. doi:10.1128/JVI.71.6.4736-4743.1997

34. Au GG, Lincz LF, Enno A, Shafren DR. Oncolytic Coxsackievirus A21 as a novel therapy for multiple myeloma. *Br J Haematol*. 2007;137(2):133-141. doi:10.1111/j.1365-2141.2007.06550.x

35. Johnson JP, Stade BG, Hupke U, Holzmann B, Riethmüller G. The melanoma progression-associated antigen P3.58 is identical to the intercellular adhesion molecule, ICAM-1. *Immunobiology*. 1988;178(3):275-284. doi:10.1016/S0171-2985(88)80071-8

36. Shafren DR, Au GG, Nguyen T, et al. Systemic therapy of malignant human melanoma tumors by a common cold-producing enterovirus, coxsackievirus a21. *Clin Cancer Res*. 2004;10(1 Pt 1):53-60. doi:10.1158/1078-0432.ccr-0690-3

37. LaRocca CJ, Warner SG. Oncolytic viruses and checkpoint inhibitors: combination therapy in clinical trials. *Clin Transl Med*. 2018;7(1):35. Published 2018 Nov 14. doi:10.1186/s40169-018-0214-5

38. Marelli G, Howells A, Lemoine NR, Wang Y. Oncolytic Viral Therapy and the Immune System: A Double-Edged Sword Against Cancer. *Front Immunol*. 2018;9:866. Published 2018 Apr 26. doi:10.3389/fimmu.2018.00866

39. Bell JC, Ilkow CS. A Viro-Immunotherapy Triple Play for the Treatment of Glioblastoma. *Cancer Cell*. 2017;32(2):133-134. doi:10.1016/j.ccell.2017.07.012

40. Hemminki O, Dos Santos JM, Hemminki A. Oncolytic viruses for cancer immunotherapy. *J Hematol Oncol*. 2020;13(1):84. Published 2020 Jun 29. doi:10.1186/s13045-020-00922-1

41. Tripodi L, Vitale M, Cerullo V, Pastore L. Oncolytic Adenoviruses for Cancer Therapy. *Int J Mol Sci*. 2021;22(5):2517. Published 2021 Mar 3. doi:10.3390/ijms22052517

42. Zheng M, Huang J, Tong A, Yang H. Oncolytic Viruses for Cancer Therapy: Barriers and Recent Advances. *Mol Ther Oncolytics*. 2019;15:234-247. Published 2019 Nov 2. doi:10.1016/j.omto.2019.10.007

43. Russell SJ. RNA viruses as virotherapy agents. *Cancer Gene Ther*. 2002;9(12):961-966. doi:10.1038/sj.cgt.7700535

44. Martinez-Quintanilla J, Seah I, Chua M, Shah K. Oncolytic viruses: overcoming translational challenges. *J Clin Invest*. 2019;129(4):1407-1418. Published 2019 Mar 4. doi:10.1172/JCI122287

45. Green NK, Herbert CW, Hale SJ, et al. Extended plasma circulation time and decreased toxicity of polymer-coated adenovirus. *Gene Ther*. 2004;11(16):1256-1263. doi:10.1038/sj.gt.3302295

46. Liu YL, Chen D, Shang P, Yin DC. A review of magnet systems for targeted drug delivery. *J Control Release*. 2019;302:90-104. doi:10.1016/j.jconrel.2019.03.031

47. Wojton J, Kaur B. Impact of tumor microenvironment on oncolytic viral therapy. *Cytokine Growth Factor Rev*. 2010;21(2-3):127-134. doi:10.1016/j.cytogfr.2010.02.014

48. Choi IK, Lee YS, Yoo JY, et al. Effect of decorin on overcoming the extracellular matrix barrier for oncolytic virotherapy. *Gene Ther*. 2010;17(2):190-201. doi:10.1038/gt.2009.142

49. Jung KH, Choi IK, Lee HS, et al. Oncolytic adenovirus expressing relaxin (YDC002) enhances therapeutic efficacy of gemcitabine against pancreatic cancer [published correction appears in Cancer Lett. 2017 Sep 28;404:93]. *Cancer Lett*. 2017;396:155-166. doi:10.1016/j.canlet.2017.03.009

50. Lemos de Matos A, Franco LS, McFadden G. Oncolytic Viruses and the Immune System: The Dynamic Duo. *Mol Ther Methods Clin Dev*. 2020;17:349-358. Published 2020 Jan 15. doi:10.1016/j.omtm.2020.01.001

51. Platanias LC. Mechanisms of type-I- and type-II-interferon-mediated signalling. *Nat Rev Immunol*. 2005;5(5):375-386. doi:10.1038/nri1604

52. Buoncervello M, Gabriele L, Toschi E. The Janus Face of Tumor Microenvironment Targeted by Immunotherapy. *Int J Mol Sci*. 2019;20(17):4320. Published 2019 Sep 3. doi:10.3390/ijms20174320

53. Najafi M, Goradel NH, Farhood B, et al. Tumor microenvironment: Interactions and therapy. *J Cell Physiol*. 2019;234(5):5700-5721. doi:10.1002/jcp.27425

54. Guedan S, Alemany R. CAR-T Cells and Oncolytic Viruses: Joining Forces to Overcome the Solid Tumor Challenge. *Front Immunol*. 2018;9:2460. Published 2018 Oct 23. doi:10.3389/fimmu.2018.02460

55. Lee WS, Yang H, Chon HJ, Kim C. Combination of anti-angiogenic therapy and immune checkpoint blockade normalizes vascular-immune crosstalk to potentiate cancer immunity. *Exp Mol Med*. 2020;52(9):1475-1485. doi:10.1038/s12276-020-00500-y

56. Bhattacharya P, Budnick I, Singh M, et al. Dual Role of GM-CSF as a Pro-Inflammatory and a Regulatory Cytokine: Implications for Immune Therapy. *J Interferon Cytokine Res*. 2015;35(8):585-599. doi:10.1089/jir.2014.0149

57. Freedman JD, Hagel J, Scott EM, et al. Oncolytic adenovirus expressing bispecific antibody targets T-cell cytotoxicity in cancer biopsies. *EMBO Mol Med*. 2017;9(8):1067-1087. doi:10.15252/emmm.201707567

58. Ishii N, Takahashi T, Soroosh P, Sugamura K. OX40-OX40 ligand interaction in T-cell-mediated immunity and immunopathology. *Adv Immunol*. 2010;105:63-98. doi:10.1016/S0065-2776(10)05003-0

59. Eriksson E, Milenova I, Wenthe J, et al. Shaping the Tumor Stroma and Sparking Immune Activation by CD40 and 4-1BB Signaling Induced by an Armed Oncolytic Virus. *Clin Cancer Res*. 2017;23(19):5846-5857. doi:10.1158/1078-0432.CCR-17-0285

60. Li X, Wang P, Li H, et al. The Efficacy of Oncolytic Adenovirus Is Mediated by T-cell Responses against Virus and Tumor in Syrian Hamster Model. *Clin Cancer Res*. 2017;23(1):239-249. doi:10.1158/1078-0432.CCR-16-0477

61. Jayawardena N, Poirier JT, Burga LN, Bostina M. Virus-Receptor Interactions and Virus Neutralization: Insights for Oncolytic Virus Development. *Oncolytic Virother*. 2020;9:1-15. Published 2020 Mar 6. doi:10.2147/OV.S186337

62. Ferguson MS, Lemoine NR, Wang Y. Systemic delivery of oncolytic viruses: hopes and hurdles. *Adv Virol*. 2012;2012:805629. doi:10.1155/2012/805629

63. Davies DH, McCausland MM, Valdez C, et al. Vaccinia virus H3L envelope protein is a major target of neutralizing antibodies in humans and elicits protection against

lethal challenge in mice. *J Virol*. 2005;79(18):11724-11733. doi:10.1128/JVI.79.18.11724-11733.2005

64. Sartor RB. Microbial influences in inflammatory bowel diseases. *Gastroenterology*. 2008;134(2):577-594. doi:10.1053/j.gastro.2007.11.059

65. Ringel Y, Maharshak N, Ringel-Kulka T, Wolber EA, Sartor RB, Carroll IM. High throughput sequencing reveals distinct microbial populations within the mucosal and luminal niches in healthy individuals. *Gut Microbes*. 2015;6(3):173-181. doi:10.1080/19490976.2015.1044711

66. Laterza L, Rizzatti G, Gaetani E, Chiusolo P, Gasbarrini A. The Gut Microbiota and Immune System Relationship in Human Graft-versus-Host Disease. *Mediterr J Hematol Infect Dis*. 2016;8(1):e2016025. Published 2016 May 1. doi:10.4084/MJHID.2016.025

67. Arumugam M, Raes J, Pelletier E, et al. Enterotypes of the human gut microbiome [published correction appears in Nature. 2011 Jun 30;474(7353):666] [published correction appears in Nature. 2014 Feb 27;506(7489):516]. *Nature*. 2011;473(7346):174-180. doi:10.1038/nature09944

68. Rinninella E, Raoul P, Cintoni M, et al. What is the Healthy Gut Microbiota Composition? A Changing Ecosystem across Age, Environment, Diet, and Diseases. *Microorganisms*. 2019;7(1):14. Published 2019 Jan 10. doi:10.3390/microorganisms7010014

69. Zitvogel L, Daillère R, Roberti MP, Routy B, Kroemer G. Anticancer effects of the microbiome and its products. *Nat Rev Microbiol*. 2017;15(8):465-478. doi:10.1038/nrmicro.2017.44

70. Garrett WS. Cancer and the microbiota. *Science*. 2015;348(6230):80-86. doi:10.1126/science.aaa4972

71. Mitra A, MacIntyre DA, Lee YS, et al. Cervical intraepithelial neoplasia disease progression is associated with increased vaginal microbiome diversity. *Sci Rep*. 2015;5:16865. Published 2015 Nov 17. doi:10.1038/srep16865

72. Chan AA, Bashir M, Rivas MN, et al. Characterization of the microbiome of nipple aspirate fluid of breast cancer survivors. *Sci Rep*. 2016;6:28061. Published 2016 Jun 21. doi:10.1038/srep28061

73. Drewes JL, Housseau F, Sears CL. Sporadic colorectal cancer: microbial contributors to disease prevention, development and therapy. *Br J Cancer*. 2016;115(3):273-280. doi:10.1038/bjc.2016.189

74. Wang T, Cai G, Qiu Y, et al. Structural segregation of gut microbiota between colorectal cancer patients and healthy volunteers. *ISME J*. 2012;6(2):320-329. doi:10.1038/ismej.2011.109

75. Shen XJ, Rawls JF, Randall T, et al. Molecular characterization of mucosal adherent bacteria and associations with colorectal adenomas. *Gut Microbes*. 2010;1(3):138-147. doi:10.4161/gmic.1.3.12360

76. Kostic AD, Gevers D, Pedamallu CS, et al. Genomic analysis identifies association of Fusobacterium with colorectal carcinoma. *Genome Res*. 2012;22(2):292-298. doi:10.1101/gr.126573.111

77. Kwa M, Plottel CS, Blaser MJ, Adams S. The Intestinal Microbiome and Estrogen Receptor-Positive Female Breast Cancer. *J Natl Cancer Inst*. 2016;108(8):djw029. Published 2016 Apr 22. doi:10.1093/jnci/djw029

78. Viaud S, Saccheri F, Mignot G, et al. The intestinal microbiota modulates the anticancer immune effects of cyclophosphamide. *Science*. 2013;342(6161):971-976. doi:10.1126/science.1240537

79. Vétizou M, Pitt JM, Daillère R, et al. Anticancer immunotherapy by CTLA-4 blockade relies on the gut microbiota. Science. 2015;350(6264):1079-1084. doi:10.1126/science.aad1329

80. Bel S, Elkis Y, Elifantz H, et al. Reprogrammed and transmissible intestinal microbiota confer diminished susceptibility to induced colitis in TMF-/- mice. *Proc Natl Acad Sci U S A*. 2014;111(13):4964-4969. doi:10.1073/pnas.1319114111

81. Zhang W, Zou G, Li B, et al. Fecal Microbiota Transplantation (FMT) Alleviates Experimental Colitis in Mice by Gut Microbiota Regulation. *J Microbiol Biotechnol*. 2020;30(8):1132-1141. doi:10.4014/jmb.2002.02044

82. Vernieri C, Casola S, Foiani M, Pietrantonio F, de Braud F, Longo V. Targeting Cancer Metabolism: Dietary and Pharmacologic Interventions. *Cancer Discov*. 2016;6(12):1315-1333. doi:10.1158/2159-8290.CD-16-0615

83. Longo VD, Fontana L. Calorie restriction and cancer prevention: metabolic and molecular mechanisms. *Trends Pharmacol Sci*. 2010;31(2):89-98. doi:10.1016/j.tips.2009.11.004

84. Crawford PA, Crowley JR, Sambandam N, et al. Regulation of myocardial ketone body metabolism by the gut microbiota during nutrient deprivation. *Proc Natl Acad Sci U S A*. 2009;106(27):11276-11281. doi:10.1073/pnas.0902366106

85. Dao MC, Everard A, Aron-Wisnewsky J, et al. Akkermansia muciniphila and improved metabolic health during a dietary intervention in obesity: relationship with gut microbiome richness and ecology. *Gut*. 2016;65(3):426-436. doi:10.1136/gutjnl-2014-308778

86. Becattini S, Taur Y, Pamer EG. Antibiotic-Induced Changes in the Intestinal Microbiota and Disease. *Trends Mol Med*. 2016;22(6):458-478. doi:10.1016/j.molmed.2016.04.003

87. Di Biase S, Lee C, Brandhorst S, et al. Fasting-Mimicking Diet Reduces HO-1 to Promote T Cell-Mediated Tumor Cytotoxicity. *Cancer Cell*. 2016;30(1):136-146. doi:10.1016/j.ccell.2016.06.005

88. Pietrocola F, Pol J, Vacchelli E, et al. Caloric Restriction Mimetics Enhance Anticancer Immunosurveillance. *Cancer Cell*. 2016;30(1):147-160. doi:10.1016/j.ccell.2016.05.016

89. Sivan A, Corrales L, Hubert N, et al. Commensal Bifidobacterium promotes antitumor immunity and facilitates anti-PD-L1 efficacy. *Science*. 2015;350(6264):1084-1089. doi:10.1126/science.aac4255

90. Konishi H, Fujiya M, Tanaka H, et al. Probiotic-derived ferrichrome inhibits colon cancer progression via JNK-mediated apoptosis. *Nat Commun*. 2016;7:12365. Published 2016 Aug 10. doi:10.1038/ncomms12365

91. Hu J, Wang C, Ye L, et al. Anti-tumour immune effect of oral administration of Lactobacillus plantarum to CT26 tumour-bearing mice. *J Biosci*. 2015;40(2):269-279. doi:10.1007/s12038-015-9518-4

92. Cai S, Kandasamy M, Rahmat JN, et al. Lactobacillus rhamnosus GG Activation of Dendritic Cells and Neutrophils Depends on the Dose and Time of Exposure. *J Immunol Res*. 2016;2016:7402760. doi:10.1155/2016/7402760

93. Aragón F, Carino S, Perdigón G, de Moreno de LeBlanc A. Inhibition of Growth and Metastasis of Breast Cancer in Mice by Milk Fermented With Lactobacillus casei CRL 431. *J Immunother*. 2015;38(5):185-196. doi:10.1097/CJI.0000000000000079

94. Gopalakrishnan V, Spencer CN, Nezi L, et al. Gut microbiome modulates response to anti-PD-1 immunotherapy in melanoma patients. *Science*. 2018;359(6371):97-103. doi:10.1126/science.aan4236

95. Routy B, Le Chatelier E, Derosa L, et al. Gut microbiome influences efficacy of PD-1-based immunotherapy against epithelial tumors. *Science*. 2018;359(6371):91-97. doi:10.1126/science.aan3706

96. Iida N, Dzutsev A, Stewart CA, et al. Commensal bacteria control cancer response to therapy by modulating the tumor microenvironment. *Science*. 2013;342(6161):967-970. doi:10.1126/science.1240527

97. Cerullo V, Diaconu I, Romano V, et al. An oncolytic adenovirus enhanced for toll-like receptor 9 stimulation increases antitumor immune responses and tumor clearance. *Mol Ther*. 2012;20(11):2076-2086. doi:10.1038/mt.2012.137

98. Callahan BJ, McMurdie PJ, Rose MJ, Han AW, Johnson AJA, Holmes SP.DADA2: High-resolution sample inference from Illumina amplicon data. *Nature Methods* 2016, 13, 581-583. doi: 10.1038/nmeth.3869

99. Mc Murdie PJ. and Holmes S. phyloseq: An R package for reproducible interactive analysis and graphics of microbiome census data. *PLoS ONE* 2013, 8:e61217.

100. Wright, E.S. Using DECIPHER v2.0 to Analyze Big Biological Sequence Data in R. The R Journal 2016, 8, 352-359

101. Schliep, K.P. phangorn: phylogenetic analysis in R. Bioinformatics 2011, 27, 592-593.

102. Hollander, M.; and Wolfe D.A. Nonparametric Statistical Methods. John Wiley & Sons. New York 1973, 115–120.

103. Dunn, O.J. Multiple comparisons using rank sums. Technometrics 1964, 6, 241-252

104. Vancomycin Treatment Increases Efficacy of Radiotherapy in Mice. *Cancer Discov*. 2020;10(2):171. doi:10.1158/2159-8290.CD-RW2019-191

105. Zagato, E., Pozzi, C., Bertocchi, A. et al. Endogenous murine microbiota member Faecalibaculum rodentium and its human homologue protect from intestinal tumour growth. Nat Microbiol 5, 511–524 (2020).

106. Wu, Menq-Rong et al. "A potential probiotic- Lachnospiraceae NK4A136 group: Evidence from the restoration of the dietary pattern from a high-fat diet." (2020).

107. Ericsson AC, Franklin CL. Manipulating the Gut Microbiota: Methods and Challenges. *ILAR J*. 2015;56(2):205-217. doi:10.1093/ilar/ilv021

108. Ley RE, Turnbaugh PJ, Klein S, Gordon JI. Microbial ecology: human gut microbes associated with obesity. *Nature*. 2006;444(7122):1022-1023. doi:10.1038/4441022a

109. Jandhyala SM, Talukdar R, Subramanyam C, Vuyyuru H, Sasikala M, Nageshwar Reddy D. Role of the normal gut microbiota. *World J Gastroenterol*. 2015;21(29):8787-8803. doi:10.3748/wjg.v21.i29.8787

110. Chiaro J, Kasanen HHE, Whalley T, et al. Viral Molecular Mimicry Influences the Antitumor Immune Response in Murine and Human Melanoma. *Cancer Immunol Res*. 2021;9(8):981-993. doi:10.1158/2326-6066.CIR-20-0814

111. Verma R, Lee C, Jeun EJ, et al. Cell surface polysaccharides of *Bifidobacterium bifidum* induce the generation of Foxp3$^+$ regulatory T cells. *Sci Immunol*. 2018;3(28):eaat6975. doi:10.1126/sciimmunol.aat6975

112. Shimura M, Nomura S, Wakabayashi M, Maruo K, Gosho M. Assessment of Hazard Ratios in Oncology Clinical Trials Terminated Early for Superiority: A Systematic Review. *JAMA Netw Open*. 2020;3(6):e208633. Published 2020 Jun 1. doi:10.1001/jamanetworkopen.2020.8633

113. Sabit H, Cevik E, Tombuloglu H. Colorectal cancer: The epigenetic role of microbiome. World J Clin Cases 2019 November 26; 7(22): 3683-3697. 10.12998/wjcc.v7.i22.3683

114. Wang Y, Zhang R, Wu D, Lu Z, Sun W, Cai Y, Wang C, Jin J. Epigenetic change in kidney tumor:downregulation of histone acetyltransferase MYST1 in human renal cell carcinoma. J Exp Clin Cancer Res 2013; 32: 8 [PMID: 23394073 DO: 10.1186/1756-9966-32-8]

115. Raskov H, Burcharth J, Pommergaard HC. Linking Gut Microbiota to Colorectal Cancer. J†Cancer†2017; 8: 3378-3395 doi: 10.7150/jca.20497